2012-11-02

Mechanism of Action Studies on a New Class of Anticancer Nucleosides

Megan E. Browning
Brigham Young University - Provo

Mechanism of Action Studies on a New Class of Anticancer Nucleosides

Megan Browning

A thesis submitted to the faculty of
Brigham Young University
in partial fulfillment of the requirements for the degree of

Master of Science

Matt A. Peterson, Chair
Gregory F. Burton
Richard G. Watt

Department of Chemistry and Biochemistry

Brigham Young University

November 2012

ABSTRACT

Mechanism of Action Studies on a New Class of Anticancer Nucleosides

Megan Browning
Department of Chemistry and Biochemistry, BYU
Master of Science

We have completed mechanism of action studies on a new class of anticancer nucleosides typified by a novel nucleoside discovered in our lab, MAP-870. In order to study the mechanism of MAP-870, several experiments were completed on a colorectal adenocarcinoma cell line, HT-29, including trypan blue cell count, sulforhodamine B assays, flow cytometry of cell cycle, propidium iodide incorporation, and phosphatidylserine externalization, Caspase-Glo3/7 assays, DNA fragmentation gel, cyclophilin A release gel, PAMPA, and confocal imaging. Sulforhodamine B assays show that MAP-870 does indeed cause growth inhibition and cell death in the model tested. PAMPA assays show that MAP-870 does not appear to enter the cell via passive diffusion. Flow cytometry showed that MAP-870 doe not appear to cause cell cycle arrest or externalization of phosphatidylserine. Caspase-Glo3/7 assays demonstrated that MAP-870 does not appear to cause caspase activation. From confocal microscopy, it appears preliminarily that MAP-870 is taken up by cells, often through pseudopodia. The mechanism of MAP-870 on cancer cells must be further studied to elucidate its mechanism of action. However, preliminarily our data could point to TGFβ as a potential target pathway involving a unique, heretofore never described, cell death mechanism.

Keywords: [anticancer nucleosides, silicon]

ACKNOWLEDGEMENTS

I'd like to thank Dr. Peterson for the project and guidance, Jadd Shelton for making so many of the compounds, Houguang Shi and Chris Cutler for vital preliminary work, the BYU chemistry department for funding, and my advisement committee for their support.

I'd also like to thank my family for their support. This thesis was written in memory of my grandfather, John Mangum, who deserves special thanks for inspiring me to be curious and to follow in his footsteps.

TABLE OF CONTENTS

ABSTRACT II

ACKNOWLEDGEMENTS III

TABLE OF CONTENTS IV

LIST OF FIGURES V

LIST OF SCHEMES VI

LIST OF TABLES VII

CHAPTER 1: INTRODUCTION 1

Type I PCD — Apoptosis *9*
Type II PCD — Autophagy *10*
Type III PCD — Necrosis *11*

CHAPTER 2: EXPERIMENTAL 15

Cell lines and culture *15*
Trypan blue cell count *15*
Sulforhodamine B assay *16*
Flow cytometry of cell cycle arrest *17*
Flow cytometry of apoptosis *18*
Caspase-Glo3/7 assay *18*
SDS-PAGE *19*
Mass spectrometry *19*
PAMPA assay *20*
Confocal imaging *21*
Statistical Analyses *21*

CHAPTER 3: RESULTS 22

MAP-870 22
Sulforhodamine B *23*
Flow cytometry *24*
Caspase activity *29*
Necrosis biomarkers *30*
Permeability of MAP-870 ..... *31*
Confocal images *33*
JRS-100 35

CHAPTER 4: DISCUSSION 37

WORK CITED 47

APPENDIX A 51

APPENDIX B 58

APPENDIX C 64

LIST OF FIGURES

Figure 1 FDA approved NDs. 2
Figure 2 MAP-870 compound structure. 5
Figure 3 Trypan blue cell count assay on HT-29 cells. 22
Figure 4 A sulforhodamine B assay of HT-29 cell treated with MAP-870. 24
Figure 5 Cell cycle measured by flow cytometry in HT-29 cells after 48 hours of treatment. 26
Figure 6 Apoptosis detection in HT-29 cells using an annexin V alexa fluor 488 conjugate and PI. 28
Figure 7 Caspase-Glo3/7 assay of HT-29 cells. 29
Figure 8 SDS-PAGE for cyclophilin A in HT-29 cells. 31
Figure 9 PAMPA permeability compared to ClogP partition coefficient.[72] 32
Figure 13 JRS-154, an N6 biotinylated derivative of MAP-870. 33
Figure 11 Preliminary confocal images. 34
Figure 12 JRS-100, a novel nucleoside with anticancer activity. 35
Figure 13 Sulforhodamine B assay determined GI_{50} of JRS-100. 36

LIST OF SCHEMES

Scheme 1 Most common mechanisms of action of NDs in cancer treatment. 4
Scheme 2 Drug discovery process modified from Lombardino and Lowe.[76] 38
Scheme 3 Working model for the MAP-870 mechanism. 39

LIST OF TABLES

Table 1 Multi-dose growth inhibition and toxicity data for MAP-870. 7
Table 2 Summary of PCD subroutines. 12

Chapter 1: Introduction

In 1953 Watson and Crick famously proposed the secondary structure of DNA.[1] In that same year, the United States Food and Drug Administration approved a derivative of one of the components of DNA as a treatment for leukemia. This derivative, mercaptopurine, is still used for cancer treatment today.[2–4] Since 1953, the four naturally occurring DNA bases (adenine, guanine, cytosine, and thymine), and their accompanying nucleosides and nucleotides have been so extensively modified that their derivatives constitute an entire class of anticancer nucleoside derivative drugs hereafter referred to as NDs. This class consists of 14 different FDA approved NDs which are shown in Figure 1.[5]

In the 1940s, it was recognized that nucleic acids were required for all cells to divide. This discovery led to the hypothesis that nucleic acid derivatives could interfere with rapidly dividing cells such as those in cancer.[6] This hypothesis, coined the antimetabolite hypothesis, led to the production and evaluation of NDs as potential drugs eventually resulting in the approval of mercaptopurine for the treatment of cancer.

Modified NDs inhibit the cellular enzymes that process nucleosides and bases thereby interfering with the cellular production and use of nucleic acids. To do this, the NDs cross the cell membrane then hinder the cellular machinery. The cellular machinery attempts to process and use the NDs as it would naturally occurring nucleotides, nucleosides, and bases; however, structural modifications on the NDs prevent them from being metabolized properly which in turn inhibits cancer cell division.

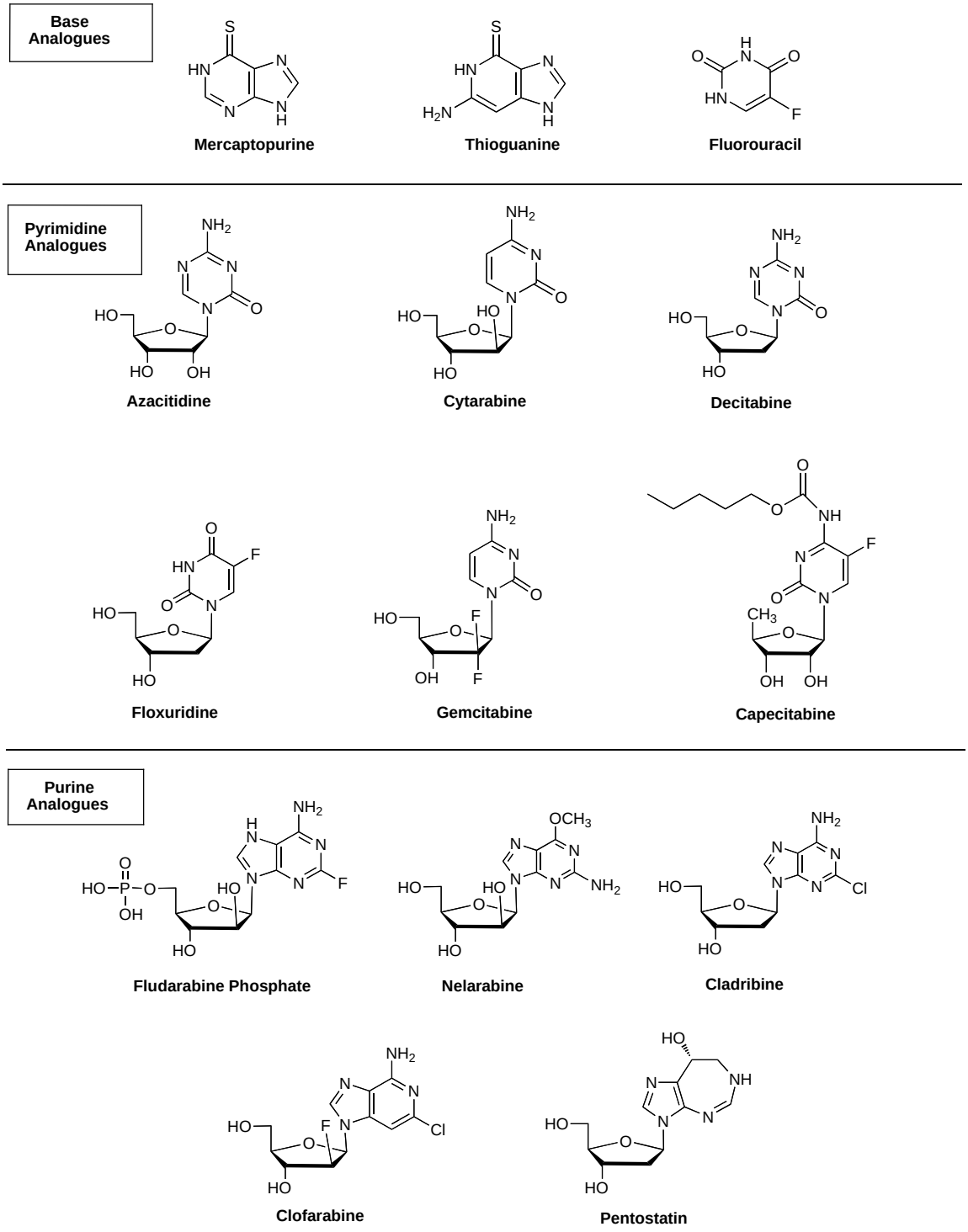

Figure 1 FDA approved NDs.

When mercaptopurine and other clinically sucessful NDs were discovered, it verified the antimetabolite hypothesis. Antimetabolites were then recognized as capable of providing effective and selective drugs. Further study showed that ideal antimetabolite drugs are small, stable, and water soluble. They must also be able to cross the cancer cell membranes either via passive diffusion or active transport. After the first drugs with activity were discovered, more NDs were designed that have these properties producing a class of antimetabolites which causes cancer cell-growth inhibition and apoptosis.

In an effort to further improve the efficacy of NDs, modifications were made to increase specificity, diminish side effects, combat resistance, and optimize pharmacokinetics. There are sevaral ways to do this. For example, a structure activity relationship (SAR) study can be used to determine what moieties on a compound are necessary for activity. Another method, called mechanism-based drug discovery involves understanding the mechanism of action NDs with anticancer activity.[7] Once the mechanism is understood, modifications can be made to the NDs to overcome any defects such as low bioavailability, non-specific binding, and side effects caused by the ND interacting with pathways that are different from those of the desired mechanism of action. Although NDs act through a variety of mechanisms, broadly speaking, NDs exert their biological effects via two general mechanisms shown in Scheme 1.[4,8]

In mechanism 1 the ND is incorporated into a growing DNA or RNA strand by a polymerase. Once incorporated, the ND either causes chain termination, destabilization of the growing strand, or inhibition of an enzyme that acts on the strand. In mechanism 2, the ND inhibits an enzyme, usually one responsible for nucleotide, nucleoside, or base metabolism, which disrupts normal cell function.

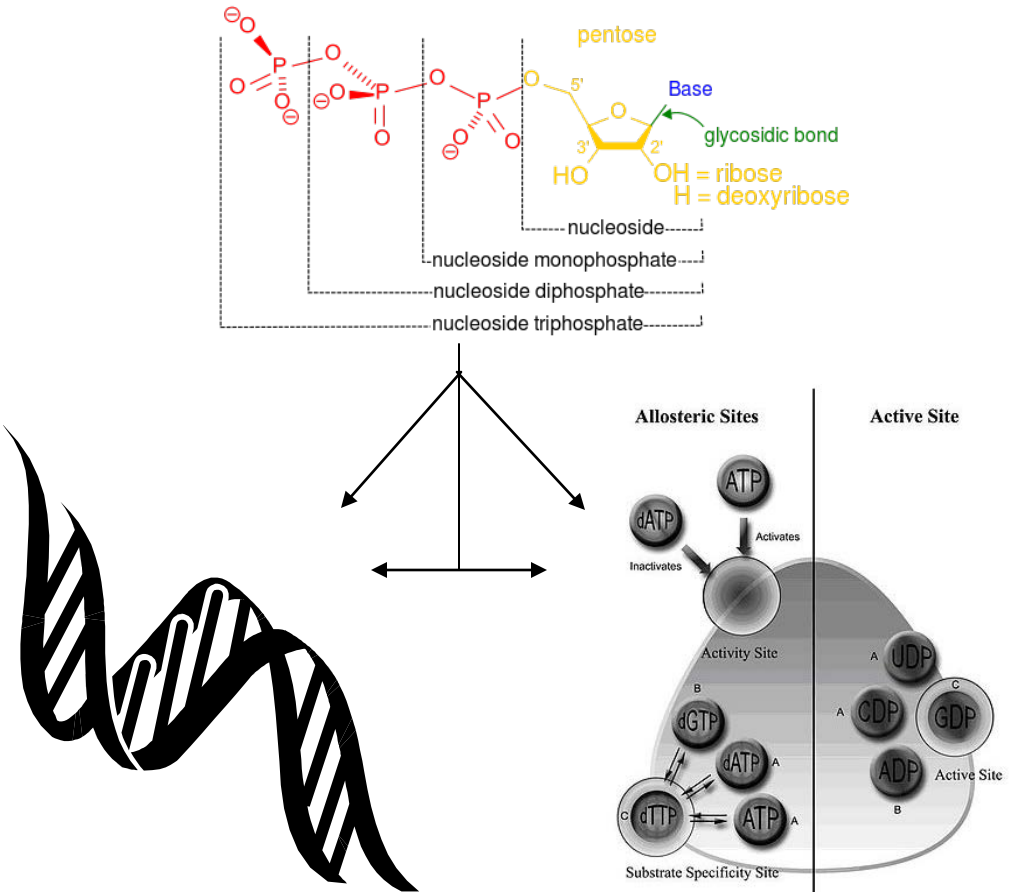

Mechanism 1 Mechanism 2

Scheme 1 Most common mechanisms of action of NDs in cancer treatment.

Mechanism 1 involves the incorporation of the ND into DNA. Mechanism 2 involves the inhibition of a biosynthesis protein (graphics from the public domain).

Examples of these mechanisms are seen in mercaptopurine and cladribine. Mercaptopurine enters cells and is converted to the riboside monophosphate by hypoxanthine-guanine phosphoribosyl transferase.[3,5] Mercaptopurine riboside monophosphate is phosphorylated to the diphosphate, and the diphosphate is reduced to mercaptopurine deoxyriboside diphosphate by ribonucleoside reductase and then phosphorylated once more to give mercaptopurine deoxyriboside triphosphate. This triphosphate is then incorporated into DNA.[5,9] Once incorporated into DNA, it causes cell cycle arrest in the mitotic phase and

apoptosis or mitotic cell death depending on the dosage.[10–12] This is in contrast to the diphosphate of cladribine which inhibits ribonucleotide reductase and causes a nucleotide pool imbalance.[13–17] This nucleotide imbalance prevents the cell from functioning properly, resulting in apoptosis.[13,18]

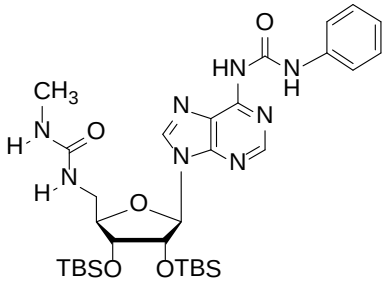

Figure 2 MAP-870 compound structure.
MAP-870 is a derivative of adenosine with TBS groups at the 2′ and 3′ OH, and further modifications at the 5′ OH and N6 of the base.

The experiments in this thesis examine an exciting potential anticancer ND, MAP-870, shown in Figure 2. MAP-870 was originally discovered during an attempt at rational drug design for an HIV reverse transcriptase inhibitor. MAP-870 was synthesized and screened for anti-HIV activity. Unfortunately, MAP-870 did not show any appreciable anti-HIV or HIV-integrase inhibitory activity at 10 μM. However, even as early as the 1960s it was well known that NDs designed to interfere with DNA did not necessarily follow expectations. This fact led to the screening of such drugs in other disease models so that active drugs were not overlooked.[6] Therefore, MAP-870 was screened for anticancer activity. The anticancer activity screen showed that MAP-870 caused unexpectedly potent cancer growth inhibition (known as cytostatic or antiproliferative activity).[19] Other NDs that had similarly unexpected results include vidarabine, gemcitabine, and zidovudine.[6] Specifically zidovudine (AZT) was originally designed as an anti-leukemia drug in the mid-1960s, however it failed cancer-drug candidate

selections at that time. Twenty years later, it was screened for in-vitro anti-HIV activity, and its antiretroviral activity was discovered.[20] AZT is now a commonly used drug in the treatment of HIV.

MAP-870 is a unique ND because of the tert-butyldimethylsilyl (TBS) groups attached to the 2′ and 3′ positions. Until fairly recently, silicon has been avoided in drug design because it was feared to be too toxic. The assumed toxicity is generally attributed to side effects from silicone breast implants. However, silicone breast implants expose the body to gram-sized doses of silicone over years, and under those conditions silicone degrades to silicon oxides that cause the aforementioned side effects.[21] As part of a larger compound, silicon has been shown to be no more intrinsically toxic than carbon.[21] The use of silicon, according to a recent review on the topic, is no cause for concern regarding potential toxicity.[21] A structure activity relationship (SAR) found that TBS groups in MAP-870 are important for potent anticancer activity.[22] When these TBS groups are replaced with esters and the compound retains antiproliferative activity, however this antiproliferative activity is decreased 3 fold.

We chose to study MAP-870 as a potential anticancer drug because of its unique structure and promising anticancer activity. The goal of this study was to better understand MAP-870 and determine the mechanism behind its anticancer activity so that more effective derivatives can be designed.

Soon after the initial discovery of the cytostatic activity of MAP-870, MAP-870 was subjected to further growth inhibition assays performed by the National Institute of Health National Cancer Institute (NIH NCI). The assay results, shown in Table 1, show that MAP-870 inhibits cell growth in almost all cell types tested and also induces specific toxicity in a majority of colon cancer cell lines and some of the renal cancer cell lines tested.[19] As the data in Table 1

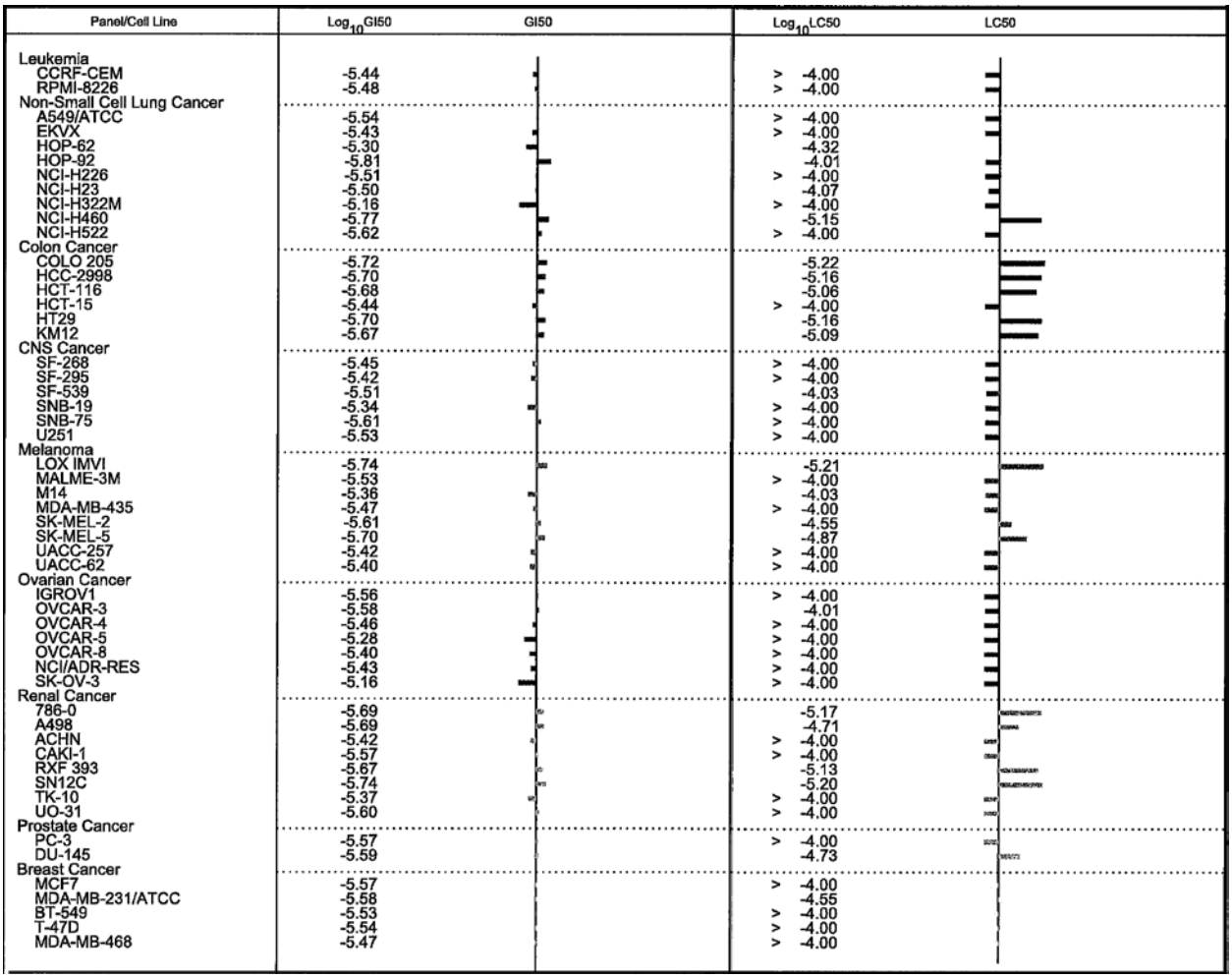

Panel/Cell Line	$Log_{10}GI50$	GI50	$Log_{10}LC50$	LC50
Leukemia				
CCRF-CEM	-5.44		> -4.00	
RPMI-8226	-5.48		> -4.00	
Non-Small Cell Lung Cancer				
A549/ATCC	-5.54		> -4.00	
EKVX	-5.43		> -4.00	
HOP-62	-5.30		-4.32	
HOP-92	-5.81		-4.01	
NCI-H226	-5.51		> -4.00	
NCI-H23	-5.50		-4.07	
NCI-H322M	-5.16		> -4.00	
NCI-H460	-5.77		-5.15	
NCI-H522	-5.62		> -4.00	
Colon Cancer				
COLO 205	-5.72		-5.22	
HCC-2998	-5.70		-5.16	
HCT-116	-5.68		-5.06	
HCT-15	-5.44		> -4.00	
HT29	-5.70		-5.16	
KM12	-5.67		-5.09	
CNS Cancer				
SF-268	-5.45		> -4.00	
SF-295	-5.42		> -4.00	
SF-539	-5.51		-4.03	
SNB-19	-5.34		> -4.00	
SNB-75	-5.61		> -4.00	
U251	-5.53		> -4.00	
Melanoma				
LOX IMVI	-5.74		-5.21	
MALME-3M	-5.53		> -4.00	
M14	-5.36		-4.03	
MDA-MB-435	-5.47		> -4.00	
SK-MEL-2	-5.61		-4.55	
SK-MEL-5	-5.70		-4.87	
UACC-257	-5.42		> -4.00	
UACC-62	-5.40		> -4.00	
Ovarian Cancer				
IGROV1	-5.56		> -4.00	
OVCAR-3	-5.58		-4.01	
OVCAR-4	-5.46		> -4.00	
OVCAR-5	-5.28		> -4.00	
OVCAR-8	-5.40		> -4.00	
NCI/ADR-RES	-5.43		> -4.00	
SK-OV-3	-5.16		> -4.00	
Renal Cancer				
786-0	-5.69		-5.17	
A498	-5.69		-4.71	
ACHN	-5.42		> -4.00	
CAKI-1	-5.57		> -4.00	
RXF 393	-5.67		-5.13	
SN12C	-5.74		-5.20	
TK-10	-5.37		> -4.00	
UO-31	-5.60		> -4.00	
Prostate Cancer				
PC-3	-5.57		> -4.00	
DU-145	-5.59		-4.73	
Breast Cancer				
MCF7	-5.57		> -4.00	
MDA-MB-231/ATCC	-5.58		-4.55	
BT-549	-5.53		> -4.00	
T-47D	-5.54		> -4.00	
MDA-MB-468	-5.47		> -4.00	

Table 1 Multi-dose growth inhibition and toxicity data for MAP-870.

This table displays profiling results for MAP-870 at multiple doses using the NCI-60 human tumor cell line screen. This profiling screen examines the effect of the probe at several concentrations on cellular growth of 60 cell lines during 48 hours of exposure using sulforhodamine B for the quantification of cellular proteins. The GI_{50} is defined as the drug concentration resulting in a 50% reduction in the net protein increase calculated as $[(T-T_0)/(C-T_0)] \times 100 = 50$, whereas the LC_{50} is the concentration of drug resulting in a 50% reduction in the measured protein at the end of the drug treatment as compared to that at the beginning calculated as $[(T- T_0)/ T_0] \times 100 = -50$ where T_0 = absorbance at time zero, C = control growth, and T = test growth in the presence of drug at the five concentration levels.[23,24] These data are displayed in a log scale both numerically and graphically below.

illustrate, MAP-870 exhibits antiproliferative activity against almost all cell types tested with an average GI_{50} (drug concentration at which cell growth is reduced 50%) of 3.13 μM. LC_{50} values (drug concentration at which 50% of the cells die) for five of the colon cancer cell lines and four of the renal cell lines ranged between 6-10 μM.[25] In comparison to a previously characterized NDs, the GI_{50} of MAP-870 is about 1/3 that of mercaptopurine which has an average GI_{50} of 11.1 μM, and the LC_{50} of MAP-870 is much lower than that of mercaptopurine which has an average LC_{50} of >100 μM (100 μM is the highest concentration tested).[26] Therefore, the potent broad spectrum antiproliferative activity of MAP-870 and cell-line specific toxicity is a strong driving force for further examination of the mechanism of action of MAP-870.

The main objective of mechanism of action studies was to determine how MAP-870 exerts its broad spectrum antiproliferative activity and selective toxicity. A first step toward achieving this goal was to determine the type of cell death caused by MAP-870. Overcoming cell death is one of the six hallmarks of cancerous cells; because cancer cells are resistant to cell death, understanding how MAP-870 induces cell death in cancer cells is vital to understanding how it induces selective toxicity.[27] Therefore, the common types of cell death are addressed below to better understand the mechanism behind MAP-870.

Programmed cell death (PCD) is cell death mediated by an intracellular program. It is classically referred to as cell-suicide or apoptosis, but recently has been redefined to include other types of cell death. PCD is commonly divided into three types, I, II, and III. These were originally distinguished by morphological features. Type I PCD, is the classic PCD also known as apoptosis that is characterized by cell rounding, retraction of pseudopodia, condensation of cytoplasm and chromatin, nuclear fragmentation, and membrane blebbing without loss of integrity.[28,29] Type II PCD is also called autophagic cell death characterized by lack of

chromatin condensation and the formation of large vacuoles called autophagosomes.[29] Type III PCD is better known as necrotic or necoptotic cell death to indicate the regulatory mechanism behind necrosis. It is characterized by cell and organelle swelling, plasma membrane permeability, and loss of intracellular contents.[2] In the lab, more definitive and quantifiable characteristics must be used to determine mechanism of cell death.

Type I PCD — Apoptosis

Type I cell death occurs naturally in organisms during development in response to excess cells no longer needed or as a line of defense against disease.[28] Pre-cancerous cells often undergo type I cell death to protect the organism from potentially harmful tumors. Apoptotic cell death is the type of cell death induced by most cancer drugs today.[27,28,30] Type I PCD proceeds via one of two pathways. These pathways are intrinsic and extrinsic depending on whether the PCD was induced intracellularly or extracellularly respectively. The intrinsic pathway occurs through the release of cytochrome *c* eventually activating caspase-9.[31] The extrinsic pathway begins via activation of membrane-bound receptors leading to cleavage of caspase-8.[31] These pathways converge as caspases-8 and -9 activate caspases-3 and -7.[31] These caspases, or cysteine-dependent aspartate-directed proteases, are good biomarkers for apoptosis. Procaspases are ever-present in the cell, and are inactive until they are cleaved upon apoptotic signals into caspases. Caspases then cleave other proteins at a DEVD amino acid sequence in a cascade; thus cleaving cellular proteins resulting in the morphological features mentioned above.

In addition to the activation of caspases, type I PCD can be characterized by phosphatidylserine (PS) exposure on the cell surface. In cellular membranes, phospholipids are distributed asymmetrically in the inner and outer leaflets.[32,33] For example, PS is a phospholipid component of the cell membrane which is normally located on the inner leaflet of the

membrane.[33,34] Early in apoptosis, caspases cleave protein kinase C8 which in turn phosphorylates scramblase. Scramblase then causes PS to "flip" so that it reorients towards the outer leaflet.[34,35] However, PS externalization has been found to occur in the absence of scramblase as well.[36] This PS externalization acts as a signal to surrounding cells to phagocytize the apoptotic cell.[32,37,38]

Apoptosis can also be identified by DNA fragmentation. Endonucleases cleave nuclear DNA in regular patterns resulting in double-stranded fragments that are 180 to 200 base pairs in length.[39] These fragments can be visualized as DNA laddering on an agarose gel.

Type II PCD — Autophagy

Type II cell death, also known as autophagic cell death, is followed by cells in a state of nutrient deficiency. In nutrient deficient conditions, Tor kinase is inactivated and a large vacuole, thought to originate from the endoplasmic reticulum, forms.[39] This vacuole, known as an autophagosome then releases its contents into lysosomes to be degraded. Through this process, cells break down their organelles into small metabolites which can be used by surrounding cells for nutrients. This is a problem if the surrounding cells are cancerous, as the dying cell then feeds surrounding tumor cells. Because of this, autophagy is a less common mechanism for cancer-treating drugs, but some examples of autophagy-causing drugs do exist.[27] Coates et al. describes cancer drugs that cause autophagy. These include tamoxifen, ionizing radiation, arsenic trioxide, temozolomide, resveratrol, rapamycin, and histone deacetylase inhibitors.[40–43] Autophagic cells have many similar characteristics to apoptotic cells. These include an intact membrane, PS exposure on the cell surface, chromatin condensation and DNA fragmentation.[36] However, autophagic cell death is not triggered by caspases, though active

caspases have been found in autophagic cells. Authophagy can be characterized by lysosomal beclin1 activation, a protein necessary for autophagosome formation.[44]

Type III PCD — Necrosis

Type III PCD (cytoplasmic cell death) or necrosis was previously thought to be unregulated and only occur through accidental cell death.[29] However, recent evidence shows that in some cases necrosis is highly regulated, for example it can be triggered by receptor stimulation in the presence of caspase inhibitors.[27,29] This regulated necrosis, often coined necroptosis, is mediated by the activity of receptor-interacting protein 1 (RIP1) kinase. This mechanism of cell death is not commonly used as a pathway for cancer treating drugs, however some experimental compounds that target this pathway have been reported.[29,30,45] Necrosis-inducing agents kill some cells and cause the cells to release their intercellular contents. The release of cellular contents in necrotic cell death also releases proinflammatory signals into the surrounding tissue, which recruits immune cells to the area. These immune cells can be actively tumor-promoting and can potentially promote angiogenesis, proliferation, and invasiveness. Necrotic cells also release cytokines that stimulate the proliferation of surrounding cells. By this logic, even though necrosis kills some cells, necrosis as a mechanism for cancer treatment may cause more harm than good.[27] However, other researchers have claimed that this activation of the immune system could be useful, and when equipped with cancer-specific antigens the immune cells could actively dispose of the remaining cells. These necrosis-inducing agents could also be combined with cancer immunovaccines for effective treatment, especially in apoptosis-resistant cells and cells that are not actively in the cell cycle.[30,46]

Necrosis is traditionally categorized by a negative result to most apoptosis and autophagy biomarkers including PS externalization, DNA strand breaks, and caspase activation, along with

early plasma membrane permeabilization.[29,45] However, very recently several cellular markers have been identified as useful for identifying necroptosis.[45] One biomarker that can be used to identify necroptosis is the release of chromatin protein high mobility group B1 (HMGB1) into the surrounding media.[45] However, this occurs in late necroptosis, and one group of researchers reasoned that if necroptosis can be identified by early plasma membrane permeabilization, then a cytosolic protein released as a result of this permeabilization could be used as a biomarker for necroptosis. Indeed, cyclophillin A, a ubiquitous, cytosolic peptidyl-prolyl *cis-trans* isomerase, is released early in necroptosis and is a reliable biomarker of necroptosis.[45] A summary of cell death characteristics is found in Table 2 below.

Table 2 Summary of PCD subroutines.

The below table is modified from Melino et al.[47]

	Type I PCD — apoptosis	**Type II PCD — autophagy**	**Type III PCD — necrosis**	**Caspase independent apoptosis**
Genetic Program	+	+	Limited	+
Membrane	Intact	Intact	Lysed	Intact
PS exposure	+	+	In late stages	+
Nucleus	Chromatin condensation and DNA fragmentation	Chromatin condensation and DNA fragmentation	No distinguishing characteristics	Chromatin condensation and DNA fragmentation
Enzymes	Caspases	Lysosomal beclin1	Limited	Calpains

Exceptions to the types of PCD mentioned above exist including anoikis, Wallerian degeneration, excitotoxicity, platelet formation, erythropoisis, cornification, and lens formation.[29,47] However, anoikis is apoptosis in response to cells detached from the extracellular matrix, Wallerian degeneration occurs in crushed nerve fibers, excitotoxicity occurs in

overstimulated nerve cells, and the other types also occur in specific cells and are probably not relevant to cancer drug treatment.[48–50] Pyroptosis and pyronecrosis occur in cells infected with bacteria, and are also probably not pertinent.[29] However, other alternative types of cell death like caspase-independent apoptosis, mitotic catastrophe, paraptosis, and entosis could pertain to the discussion of the MAP-870 mechanism.

Caspase-independent apoptosis has been best characterized in cells with genetically or pharmacologically neutralized caspases.[51] For example, potential cancer-treating drugs including Honokiol, Sorafenib, 7-beta-hydroxycholesterol, and 7-ketocholesterol cause apoptosis even in the presence of caspase inhibitors. All of these drugs activate caspases in untreated cells, and treatment with caspase inhibitors does not necessarily indicate a shared mechanism of caspase-independent cell death.[51–54]

Mitotic catastrophe has been shown to occur with some cancer treating drugs, and has been reported as a mechanism for several nucleoside drugs including mercaptopurine and fluorouracil. This occurs at lower doses, while at higher doses these drugs cause apoptosis.[12,55]

Parapotosis has only been recorded in cells over-expressing insulin-like growth factor receptor I.[29,56,57] It is characterized by cytoplasmic vacuolization and mitochondrial swelling, and is not positive for apoptotic biomarkers.[29]

Entosis is a type of cellular cannibalism seen in the lymphoblasts of patients with Huntington's disease, but also occurs in cancer cells that lack cell death inducing proteins like MCF-7 breast cancer cells, which lack caspase-3 and beclin-1 making them resistant to both apoptosis and autophagy.

Determining the method of cell death by which MAP-870 exerts its broad antiproliferative activity and specific cytotoxicity, will lay a foundation that will ultimately allow

us to better understand the mechanism and how to improve its activity. MAP-870 could potentially be an effective colon cancer treatment, and with over 50,000 colon cancer deaths in 2011, promising new treatments must be pursued.[58]

Chapter 2: Experimental

Cell lines and culture

HT-29 and H23 cells were obtained from the laboratory of Professor Kim O'Neil (Department of Microbiology & Molecular Biology, Brigham Young University). The cells were grown in McCoy's 5A medium modified (Sigma). COLO-205 cells were obtained from the laboratory of Professor Marc D. Hansen (Department of Physiology & Developmental Biology, Brigham Young University) and were grown in RPMI medium (Sigma). HEK293T and HeLa cells were obtained from the laboratory of Professor Barry Willardson (Department of Chemistry and Biochemistry, Brigham Young University) and were grown in 50:50 Dulbecco's Modified Eagle's Medium/Nutrient F-12 Ham (Sigma). All media were supplemented with 10% fetal bovine serum (Sigma), 2.8 mM L-glutamine (Gibco), and 50 mg/L of gentamicin (Sigma). The cells were incubated at 37 ºC with 5% CO_2 in a NuAire incubator. The cells were subcultured regularly in order to maintain active growth.

Trypan blue cell count

In 3 mL medium on a six well plate (Starstedt), 0.25 million cells per well were plated, and soon after treated with 1% DMSO as a vehicle control, camptothecin (Sigma) as a positive control, or 10 μM MAP-870 and incubated for 48 hours. Cells were rinsed with PBS, then trypsinized with 0.05% trypsin (Gibco), and suspended in PBS (Fisher Scientific). Cells were counted as per Freshney.[59] In short, the cell suspension was vortexed, and 2 μL of the cell suspension was added to 98 μL of trypan blue (Sigma) and mixed by pipetting up and down. Next, 10 μL of the cell suspension/trypan blue mixture was pipetted onto a hemocytometer, covered with a glass slide, and counted using a light microscope. Nine squares on the hemocytometer were counted and averaged, and the number of cells was determined by

multiplying this number by the dilution, 50, and the volume, 10^4. When counting live cells, as in Figure 3, the cells without trypan blue stain incorporated were counted, however during routine passaging live cells without trypan blue incorporation were counted.

Sulforhodamine B assay

Ten thousand cells per well were plated in 100 µL medium on clear 96-well plates (Grenier Bio-One), treated with 0.1% DMSO as a vehicle control, camptothecin (Sigma) as a positive control, or 100 µM, 50 µM, 25 µM, 10 µM, or 5 µM of MAP-870 or JRS-100, and incubated at 37 °C for 48 hours. The total DMSO concentration on cell cultures did not exceed 0.1%. Cell density was measured using a sulforhodamine B based *in vitro* toxicology assay kit (Sigma). Cells were fixed by adding 100 µL of 50% TCA, and incubating at 4 °C for 1 hour. TCA was removed, and the fixed cells were washed, and 150 µL Sulforhodamine B Solution [0.4%] was added to the fixed cells and allowed to incubate at RT for 25 minutes. Cells were then washed with 1% acetic acid. Incorporated sulforhodamine B was solubilized in 10 mM Tris, and allowed to stand at RT for 5 minutes. The sulforhodamine-Tris solution was transferred to a new clear 96-well plate (Grenier Bio-One), and absorbance was measured with the Synergy H4 plate reader (BioTek) at 565 nm.

Calculations:

The GI_{50} is the concentration of test drug which satisfies equation 1.[23]

Equation 1

$$\frac{T - T_0}{C - T_0} \times 100 = 50$$

T = optical density of the test well after a 48-h period of exposure to test drug
T_o = the optical density at time zero
C= the control optical density

The LC_{50} is the concentration of drug where equation 2 is true, and when enough cells have died so that the absorbance after treatment is half of the absorbance before treatment, hence the -50 in the equation below.[23]

Equation 2

$$\frac{T - T_0}{T_0} \times 100 = -50$$

T = optical density of the test well after a 48-h period of exposure to test drug
T_o = the optical density at time zero

Flow cytometry of cell cycle arrest

In a 3 mL medium on a six well plate (Starstedt), 0.25 million cells per well were plated, and soon after treated with 0.1% DMSO as a vehicle control, 10 μM camptothecin (Sigma) as a positive control, or 100 μM, 50 μM, 25 μM, 10 μM, or 5 μM of MAP-870 and incubated for 48 hours. The total DMSO concentration on cell cultures did not exceed 0.1%. Cells were rinsed with PBS, then trypsinized with 0.05% trypsin (Gibco), and suspended in PBS (Fisher Scientific). The suspension and the PBS rinsing were added to the decanted media to include detached cells. The cells were centrifuged at 300 x g for 5 minutes, the supernatant was decanted, and the cells were resuspended in 0.5 mL of PBS. To fix the cells, 4.5 mL of ice cold 70% ethanol was added, and the cells were stored at 4ºC for 24 hours. After fixation, the cells were again centrifuged for 5 minutes at 300 x g. The supernatant was decanted, and the cells were resuspended in 5 mL of PBS, and after 30 s were centrifuged at 300 x g for 5 minutes. The supernatant was decanted, and the cells were resuspended in a propidium iodide (PI) staining solution consisting of 0.1% Triton X-100 (Fischer Scientific), 10 ug/mL propidium iodide (AnaSpec), and 100 ug/mL DNase-free RNase A (Sigma) in PBS. The stained cells were incubated in the dark for 30 minutes at room temperature, then PI fluorescence was measured

using a FACSCanto flow cytometer (BD Biosciences), excited at 488 nm and detected at 585 nm.[60]

Flow cytometry of apoptosis

In 3 mL of media on a six well plate (Starstedt), one million cells per well were plated, and soon after treated with 0.1% DMSO as a vehicle control, 10 μM camptothecin (Sigma) as a positive control, or 10 μM of MAP-870 and incubated for 12 hours. The total DMSO concentration on cell cultures did not exceed 0.1%. Cells were rinsed with PBS, then trypsinized with 0.05% trypsin (Gibco), and suspended in PBS (Fisher Scientific). The suspension and the PBS rinsing were added to the decanted media to include detached cells. The cells were centrifuged at 300 x g for 5 minutes, the supernatant was decanted, and the cells were resuspended in 0.1 mL of annexin binding buffer (10 mM HEPES, 140 mM NaCl, 2.5 mM $CaCl_2$, pH 7.4). Next, 5 μL of an annexin V, alexa fluor 647 conjugate (Invitrogen) was added and incubated at room temperature for 15 minutes in the dark. After incubation, 400 μL more of the annexin binding buffer and 5 μL of 1 mg/mL PI were added. After another 5 minute incubation in the dark, the cells were analyzed using a FACSCanto flow cytometer (BD Biosciences), excited at 488 nm and detected at 585 nm for PI and excited at 633 nm and detected at 670 nm for the an annexin V, alexa fluor 647 conjugate.[60]

Caspase-Glo3/7 assay

Ten thousand cells per well were plated in 100 μL medium on white 96-well plates (Grenier Bio-One), treated soon after with 0.1% DMSO as a vehicle control, camptothecin (Sigma) as a positive control, or 100 μM, 50 μM, 25 μM, 10 μM, or 5 μM of MAP-870, and incubated at 37 °C for 48 hours. The total DMSO concentration on cell cultures did not exceed

0.1%. Apoptosis was measured using a Caspase-Glo3/7 assay kit (Promega). The Caspase-Glo3/7 assay is a luminescent assay that measures caspase-3 and caspase-7 activity. The Caspase-Glo3/7 assay mixture first causes cell lysis; then a component of the mixture is cleaved. This cleavage results in a luminescent signal, which is proportional to the amount of caspase present. Luminescence was measured after 60 minutes as per the protocol (Promega) and recorded using the Synergy H4 plate reader (BioTek).

SDS-PAGE

Cells were treated with 10 μM MAP-870 for 48 hours, and then the cell media supernatant was collected and concentrated the media using 10 kDa concentrators (Millipore). A 20 μL aliquot of the concentrated sample was added to 5 μL 5x loading dye and incubated at 95 ºC for 5 minutes. The samples were then loaded onto a 15% SDS-PAGE gel.[61] The gel was run at 15 mA until proteins moved through the stacking phase, then 20 mA until the tracking dye neared the bottom. The gel was stained using gelCode Blue Stain Reagent (Thermo Fisher Scientific) by washing the gel in deionized water three times 5 minutes each then immersing it in stain reagent for 1-2 hr. Then the stain reagent was decanted and the gel was immersed in a 50/10 destaining solution overnight.

Mass spectrometry

Gel bands of 10 kDa - 50 kDa were excised and the protein was purified and concentrated using 10k concentrators (Millipore) and the in gel FASP protocol optimized in the laboratory of Professor John T. Prince (Department of Chemistry and Biochemistry, Brigham Young University).[62] Mass Spectrometry was performed on a Thermo LTQ Orbitrap by staff working in the laboratory of Professor John T. Prince.

PAMPA assay

The pre-coated PAMPA plate system (BD Gentest) was warmed to room temperature for at least 30 minutes. Stock solutions of 100 μM MAP-870 or solutions of control compounds were prepared by diluting stock solutions into 5% ethanol in PBS. The 5% ethanol in PBS was verified for compatibility with the membrane using lucifer yellow, which is known to not pass through a PAMPA membrane. The membrane permeability was still intact with 5% ethanol in PBS, and it also could dissolve highly insoluble MAP-870. To the receiver plate, 300 μL of compound solutions per well were added, and 200 μL of 5% ethanol in PBS were added per well to the filter plate. The filter plate was lowered onto the receiver plate, and the entire assembly was incubated at room temp for 5 hours. After incubation, the solutions were transferred to UV transparent plates (Grenier Bio-One) and compound concentrations were determined by absorbance on a Synergy H4 plate reader (BioTek) at 260 nm. The permeability of each compound was calculated using equations 3 and 4 below from the BD Gentest protocol.

Equation 3

$$P_e = \frac{-ln[1 - \frac{C_A(t)}{C_{equilibrium}}]}{A \times (\frac{1}{V_D} + \frac{1}{V_A}) \times t}$$

Equation 4

$$C_{equilibrium} = \frac{C_D(t) \times V_D + C_A(t) \times V_A}{V_D + V_A}$$

$C_D(t)$ = compound concentration in donor well at time t. (mM)
$C_A(t)$ = compound concentration in acceptor well at time t. (mM)
V_D = donor well volume = 0.3 mL
V_A = acceptor well volume = 0.2 mL
A = filter area = 0.3 cm^2
t = incubation time = 18000 s (= 5 hr)

Confocal imaging

HT-29 cells were seeded at 0.2 million cells / mL in 4 well Lab-Tek® II Chamber Slides™ (Electron Microscopy Sciences). Cells were treated with JRS-154, a biotinylated MAP-870, and incubated for 48 h. JRS-154 concentrations were verified using UV-vis spectroscopy (Beckman-Coulter Inc. DU730 life sciences UV-Vis spectrometer). After 48 h, cells were fixed inspected under a light microscope and rinsed with PBS (Fisher Scientific). Cells were fixed in 4% paraformaldehyde (Sigma Aldrich) for 15 min. Cells were rinsed again in PBS, and then permeabilized for 7 min with 0.5% triton X-100 (Fisher Scientific). Cells were washed 3 times (at least 5 min each) in PBS. A 1:500 dilution of avidin alexa fluor 488 conjugate (Invitrogen) in PBS was incubated over the slides for 60 min at RT protected from light. After incubation, slides were washed again 3 times (at least 5 min each) with PBS. Slides were mounted using mounting media with DAPI (Vectashield). Cells were visualized using an Olympus FluoView FV 300 confocal laser scanning microscope. Fluorophores were excited at 458 nm 488 nm.

Statistical Analyses

Statistical analyses including averages, standard deviations, f tests, t tests, linear regression lines, and graphs were calculated using Microsoft Excel 2002 (version 10.2614.2625; Microsoft Corporation). Flow cytometry data was analyzed using FACSDiva Version 6.1.3 and further assessed for cell cycle arrest using ModFit LT.

Chapter 3: Results

MAP-870

Preliminary studies were performed in order to demonstrate that MAP-870 has a similar toxicity in our lab as in experiments performed by the NCI. Initially, this was tested by using a simple trypan blue cell count assay in colon cancer cell line, HT-29. According to statistical analyses done on the raw data, the no treatment and 1% DMSO cell counts are the same with a 95% confidence. In addition, the 10 µM MAP-870 treated cell count is different than both the no treatment and 1% DMSO cell counts with a 95% confidence interval as shown in Figure 4. However, it has been previously shown that the vehicle, DMSO, can be toxic to cells. For this reason, it was concluded that DMSO concentrations should be minimized, therefore a more concentrated MAP-870 stock solution was used and the DMSO concentration was reduced to less than 0.1%.

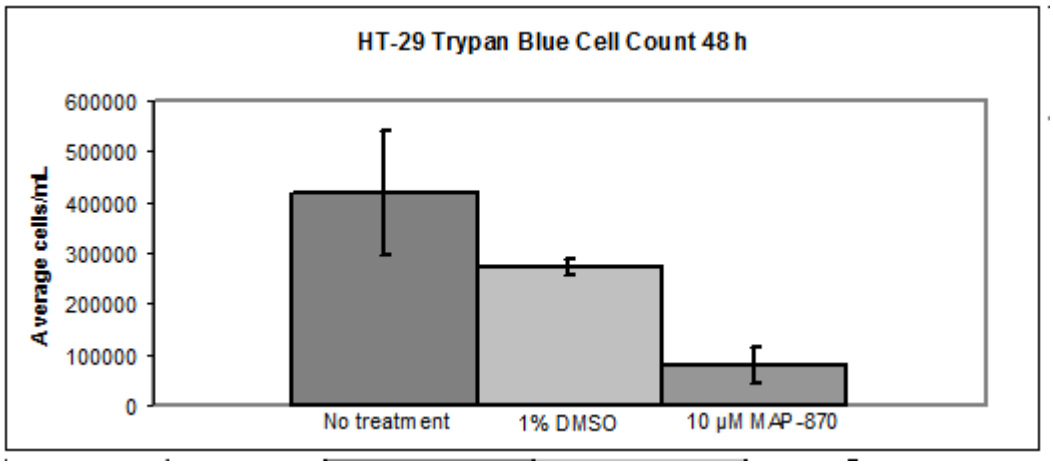

Figure 3 Trypan blue cell count assay on HT-29 cells.
The concentration of trypan blue negative cells in cells/mL (y-axis) was plotted against the treatment (x-axis). The cells were plated and treated for 48 h before being collected and counted using trypan blue. The number of cells counted per square varied from 0-37. Error bars represent one standard deviation (n=3). With 95% confidence two sample t-test the no treatment and 1% DMSO data are the same (P=0.17). Both are different than the 10 µM MAP-870 (P=0.0046 and P=0.00052, respectively).

Sulforhodamine B

Cell growth assays similar to those performed by the NCI were repeated in HT-29 using sulforhodamine B as a colorimetric assay for cellular proteins. This assay is used by the NCI to determine the GI_{50} of potential candidate drugs. Sulforhodamine B is a fluorescent dye that binds to proteins in the cells under mildly acidic conditions. After washing, sulforhodamine B desorbs from the proteins when treated with mildly basic conditions and can thus be extracted from the cells.[63] The extracted sulforhodamine B absorbs light proportional to the total protein present in the well, which is proportional to the number of cells present. In the colon cancer cell line tested, MAP-870 caused a decrease in cellular proteins in cultured cells which is indicative of growth inhibition in a dose-dependent manner as shown in Figure 4. The GI_{50} of MAP-870 in HT-29 cells was determined to be 18 ± 3 μM whereas the GI_{50} found by the NIH was 4.6 ± 1 μM.[22] In addition, the LC_{50} of MAP-870 in HT-29 cells was 42 ± 4 μM while the NIH reported an LC_{50} of 6.9 μM.[22] Using a two sample t test, it was determined that with 95% confidence that the experimental data obtained in our lab and the NIH data is different (P=0.00045). The discrepancies in the above data may be due to a poor curve fit used to determine experimental values, differences in experimental procedure, and the poor solubility of MAP-870. Although our results were higher than those obtained by the NIH, MAP-870 treatment did cause a decrease in cellular proteins in a dose-dependent manner. We concluded that the dose-responsive growth inhibition and cell death determined in our hands supported the use of HT-29 as an adequate model for future mechanistic experiments in our lab.

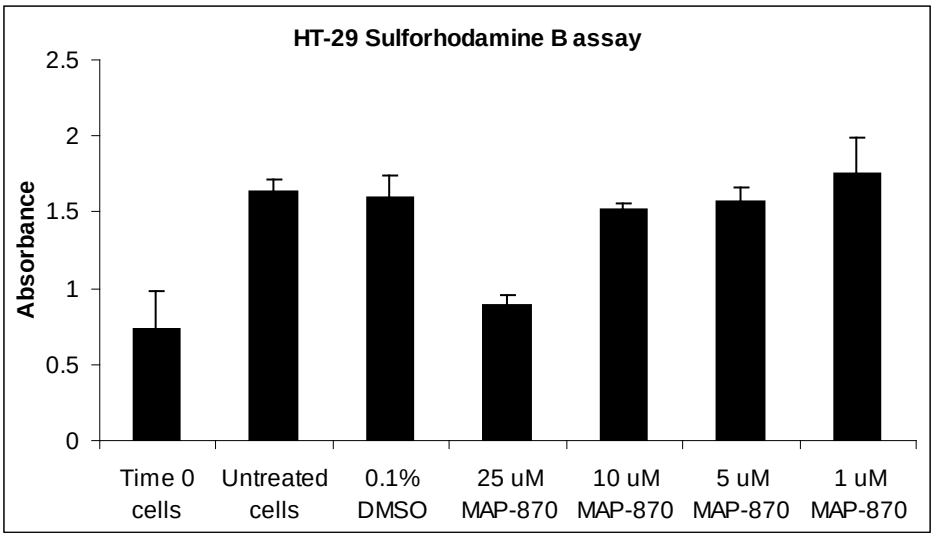

Figure 4 A sulforhodamine B assay of HT-29 cell treated with MAP-870.

Cells were treated for 48 h. The absorbance of sulforhodamine B (y-axis) was plotted against the treatment (x-axis). The cells were plated and treated for 48 h before being collected and the proteins were quantified using sulforhodamine B. The bars represent one standard deviation (n=6). GI_{50} values were derived from this data by curve fitting all optical densities for the six runs at each concentration. A linear regression line was used and the 50% absorbance of the vehicle control was obtained via interpolation.

Flow cytometry

Flow cytometry was used to determine if MAP-870 was causing cell death via a mechanism involving apoptosis and cell cycle arrest like a majority of previously-studied anti-cancer NDs. Cells were treated with MAP-870 for up to 48 hours and then fixed and stained with propidium iodide (PI). Flow cytometry was then used to count the cells individually and detect the amount of PI in each cell. The amount of PI in the cells is proportional to the amount of DNA in the cells and is indicative of what stage of the cell cycle the cell is in at the time of fixation. When a cell first divides, it has only one copy of its genome, but over time it makes a second copy so that when it divides one copy can go to each cell. When the cell has one copy, it is in G1. As the cell synthesizes a second copy it is in in S phase. The final stage is short in which the cell has two copies of the genome before it divides, called G2. The amount of DNA in cells in G2 phase is twice that of G1, and cells in the S phase have an intermediate amount of

DNA. In addition, cells that are non-viable and cell fragments appear with only a small amount of detectable DNA.

In colon cancer HT-29 cells, there was a drastic increase in cellular debris from wells with cells treated with MAP-870 compared to vehicle (0.1% DMSO) treated wells in 3 separate runs. Wells containing another colon cancer cell line, Colo-205, exhibited cellular debris as well (data not shown), but not as significantly as HT-29 possibly because in Colo-205 some of the cells are adherent and some are in suspension, and the two different phenotypes may interact with the compound differently.

Figure 5 shows that cells treated with 25 μM MAP-870 for 48 hours had an increase in aggregates and debris (cells with a different amount of DNA than the cell cycle peaks) compared to cells treated with the vehicle control; however, the live cells in G1, G2 and S phase appear to be very similar between 25 μM MAP-870 treated and vehicle control treated control cells. The raw data can be seen in Appendix A. Therefore, it appears from Figure 5 that MAP-870 does not seem to cause cell cycle arrest. The positive control, camptothecin, is a known apoptosis inducer that causes cell cycle arrest in the G2 phase.[64,65] This can be seen in Figure 5, demonstrating that the experiment worked even if negative results for MAP-870 were obtained.

Alternatively, MAP-870 may cause cell death quickly and any cells that took up MAP-870 can be found in the debris and agregates whereas the cells remaining have not yet taken up MAP-870 and are thereby the same as the untreated cells. This could also explain the increase in debris and agregates the 25 μM MAP-870-treated wells.

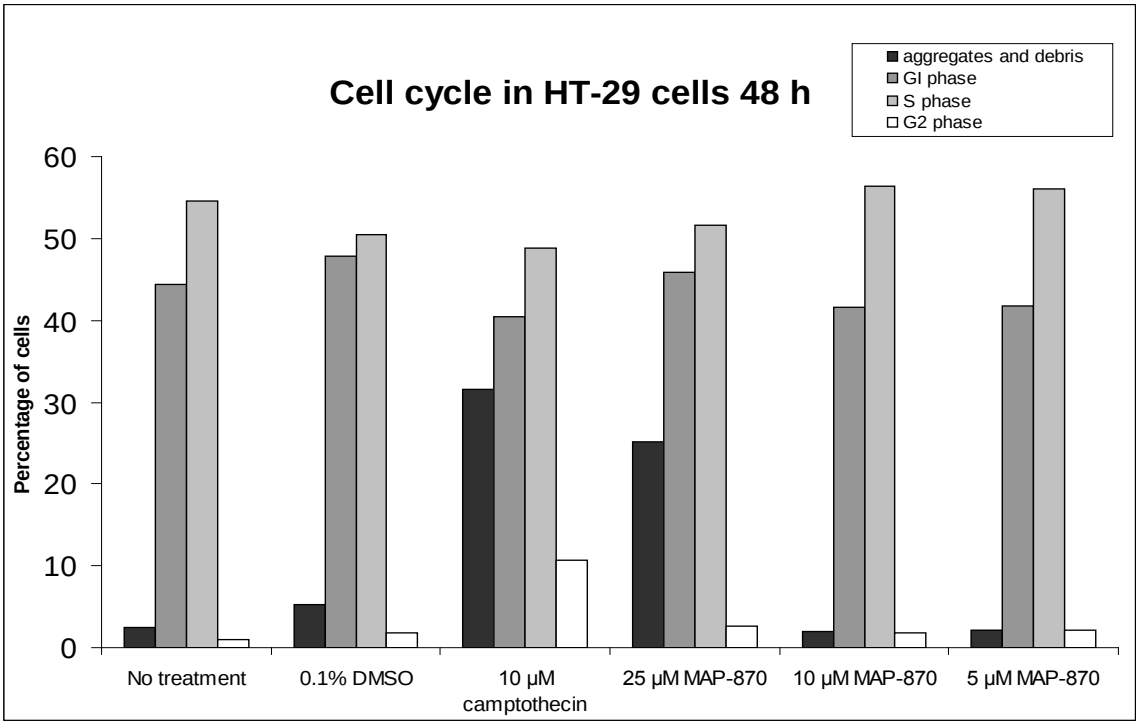

Figure 5 Cell cycle measured by flow cytometry in HT-29 cells after 48 hours of treatment. The percentage of cells (y axis) is plotted against the treatment (x axis). The percentage for G1, S, and G2 phase cells is the percentage of total live cells, while the aggregates and debris is the percentage of total cells counted. 0.5 million HT-29 cells were plated and treated and then incubated for an additional 48 h. Propidium iodide staining was performed and 10,000 counts of each sample were analyzed by flow cytometry. Data was processed using ModFit LT.

This lack of cell cycle arrest is interesting because many anticancer NDs cause cell cycle arrest prior to causing type I PCD (apoptosis).[11] The interesting flow cytometry results led to the question of how much and in what ways the mode of action of MAP-870 differs from that of other anti-cancer NDs. Because type I PCD is the most common mechanism of cell death among FDA approved anti-cancer NDs,[11,66] an assay for type I PCD was performed.

To test for type I PCD, flow cytometry was again used. In normal cells, phospholipids are arranged asymmetrically on the inside and outside of cell membranes. Usually phosphatidlycholine and sphingomyelin are exposed on the extracellular surface, and phosphatidylserine (PS) is on the cytosolic inner surface. During apoptosis PS is flipped so that

it is exposed to the outer surface. This pathway is utilized to identify apoptotic cells by using a PS binding protein, annexin V, an anticoagulant protein covalently bound to a fluorescent conjugate.[34]

Cells stained with this conjugate can be examined by flow cytometry to distinguish types of cell death. In addition to the annexin V conjugate, the cells were also stained with PI. PI was used above for the cell cycle arrest experiments. PI is cannot permate the cell membrane, but in cell cycle arrest assays the cells were fixed and their membranes permeabilized so that PI could pass into the nucleus allowing for the quantification of cellular DNA. However in this experiment, PI is used as a qualitative marker distinguishing cells with permeable membranes from those without, so the cells examined are not fixed or permeabilized. Cells undergoing types I, II, and III PCD demonstrate PS externalization, however, type III PCD cells demonstrate early PI permeabilization in addition to PS externalization, so this assay allows for distinguishing between multiple types of PCD.[67] The results this method can distinguish between include: non-apoptotic or viable cells (annexin-/PI-), early apoptotic cells (annexin+/PI-), late stage necrotic cells/late stage apoptotic cells (annexin+/PI+), and necrotic cells (annexin-/PI+).[31,67,68]

The raw data for one flow cytometry experiment is shown in Appendix B and the summary of three flow cytometry experiments is shown in Figure 6. Camptothecin is used as a positive control, because it has been shown to cause apoptosis by topoisomerase I inhibition. In addition, camptothecin is recommended by BD Biosciences as a positive control for apoptosis assays.[69] Using the data in Figure 6, a set of two-tailed sample T tests determined that the 0.1% DMSO treated cells were the same as the 10 μM camptothecin treated cells for the necrotic cell subpopulation and were different for other two populations, indicative of an increase in apoptotic cells with a 95% confidence. In addition, another set of two-tailed sample T tests showed that

there was not statistically significant difference between the 0.1% DMSO treated cells and those treated with MAP-870 for all these subpopulations (confidence level = 95%). Therefore, there is no appreciable difference in PS exposure or PI permeability between treated cells and the vehicle control. These results led us to believe that MAP-870 does not cause PS exposure or membrane permeabilization, and appears to not cause standard type I, II, or III PCD.

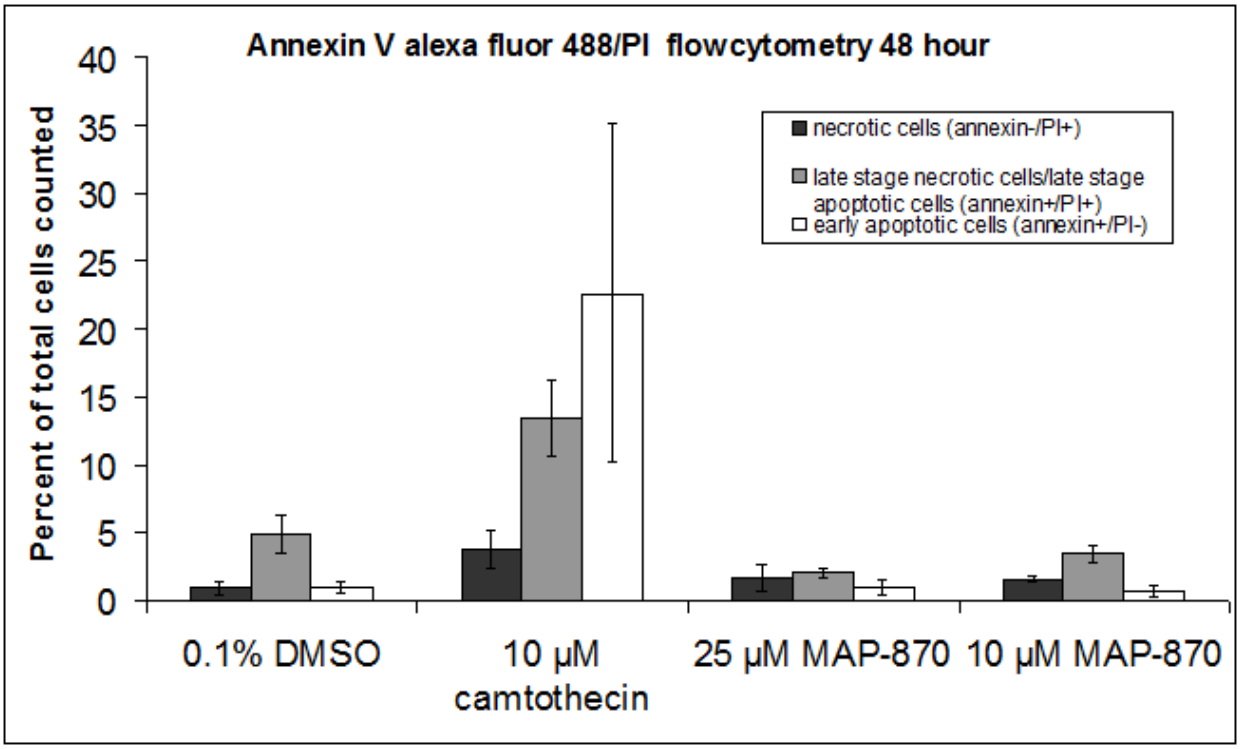

Figure 6 Apoptosis detection in HT-29 cells using an annexin V alexa fluor 488 conjugate and PI.

The percentage of cells (y axis) is plotted against the treatment (x axis). 0.5 million HT-29 cells were plated and treated and then were incubated for an additional 48 h. Propidium iodide and annexin V alexa fluor 488 conjugate staining was performed and 50,000 counts of each sample were analyzed by flow cytometry. The analyses were run in triplicate and error bars represent standard deviation. The white bars represents cells that tested positive for annexin V but negative for PI staining, early apoptotic cells. The light grey represents cells that tested positive for both annexin V and PI, cells that are either in late stage necrosis, apoptosis, or dead. The dark grey represents cells that are positive for PI but not annexing V, cells undergoing necrosis.

Caspase activity

In order to further investigate whether MAP-870 causes type I PCD, a caspase activity assay was performed. The Caspase-Glo3/7 assay kit from Promega includes a substrate DEVD sequence covalently attached to a luciferin moiety. If activated caspases are present, they cleave the substrate thereby releasing luciferin. Luciferin is in turn cleaved by luciferases present in the Promega assay mixture producing a luminescent signal proportional to the amount of caspase present. Figure 7 shows the assay results using several MAP-870 concentrations. The figure demonstrates a positive response in cells treated with camptothecin, a known apoptosis inducer, and no evidence of caspase activation or caspase-driven type I PCD. This is the second support that MAP-870 does not appear to cause type I PCD.

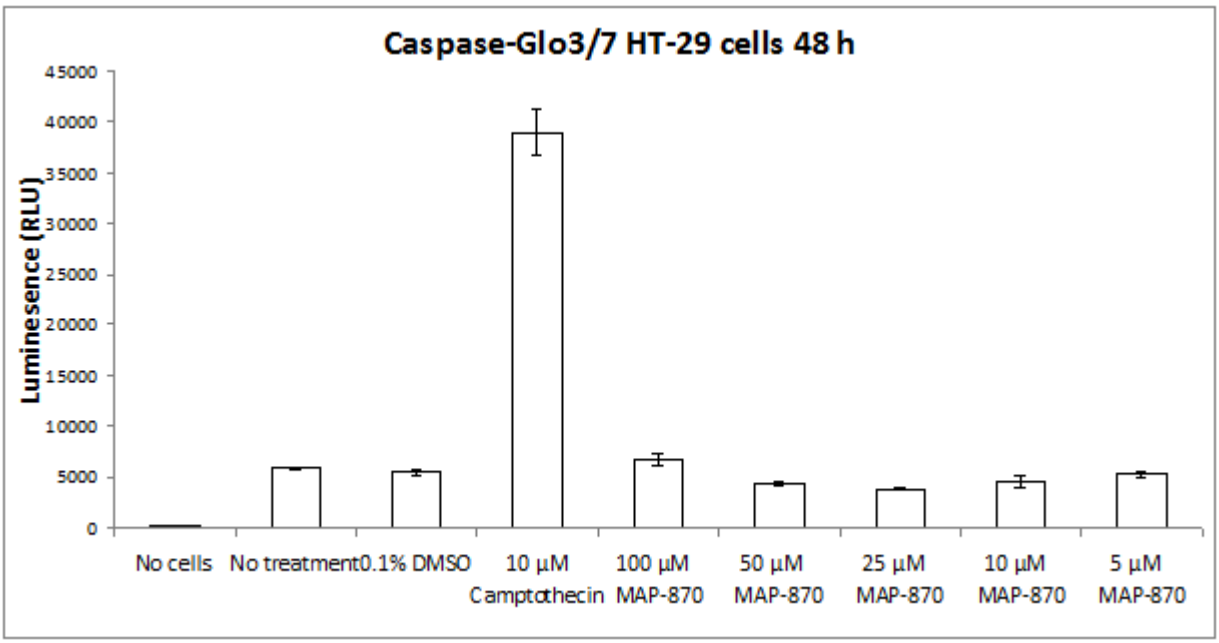

Figure 7 Caspase-Glo3/7 assay of HT-29 cells.

The luminescence in relative luminescence units (RLU) (y-axis) is plotted against the cell treatment (x-axis). 10,000 HT-29 cells were plated and treated and then incubated for an additional 48 h. 48 h was chosen for consistency with the previous sulforhodamine B and flow cytometry assays. After 48 h, the cells were treated with the caspase-glo3/7 mixture from Promega and caspase activity was detected as luminescence from the caspase-cleavage product.

Necrosis biomarkers

Of the three standard types of cell death (PCD types I, II, and III) experiments conducted up to this point in the project suggested that MAP-870 did not cause any of these.[29] However, within these three main PCD types there are subtypes, and there are also atypical cell death modalities which do not follow the pattern of any of the three standard types of cell death. The assays above did not show evidence of MAP-870 causing caspase-activated type I PCD, so the next test performed was for a type III PCD biomarker. Type III PCD was originally defined as unregulated cell death, but has since been found to have distinct cell markers. An example of such cell markers are cyclophilins. For example, cyclophilin D controls mitochondrial membrane permeability in necrotic cell death.[29] More recently, it has been found that cyclophilin A is released from cells early in necrosis upon membrane permeabilization and can be used to characterize necrosis.[45] In an effort to test for the presence of cyclophilin A in the supernatant media of HT-29 cells treated with 10 μM MAP-870, medium was collected from treated cells, concentrated, and run on an SDS-PAGE as shown in Figure 8. If type III PCD was occurring, a band for cyclophilin A was expected at 17 kDa, however there is no visible band present. This could be because the stain used to visualize the gel was Coomassie Brilliant Blue, and in the literature Christofferson and Yuan used a more sensitive silver stain to visualize cyclophilin A in their SDS-PAGE gel.[45] To determine if cyclophilin A was in fact present despite the insensitivity of the Coomassie stain, mass spectrometry was used to detect cyclophilin A. On a similarly run unstained gel, gel slices from 5 kDa to 60 kDa were cut from the gel and analyzed by mass spectrometry. In the excised gel slices, no cyclophilin A was detected (data not shown).

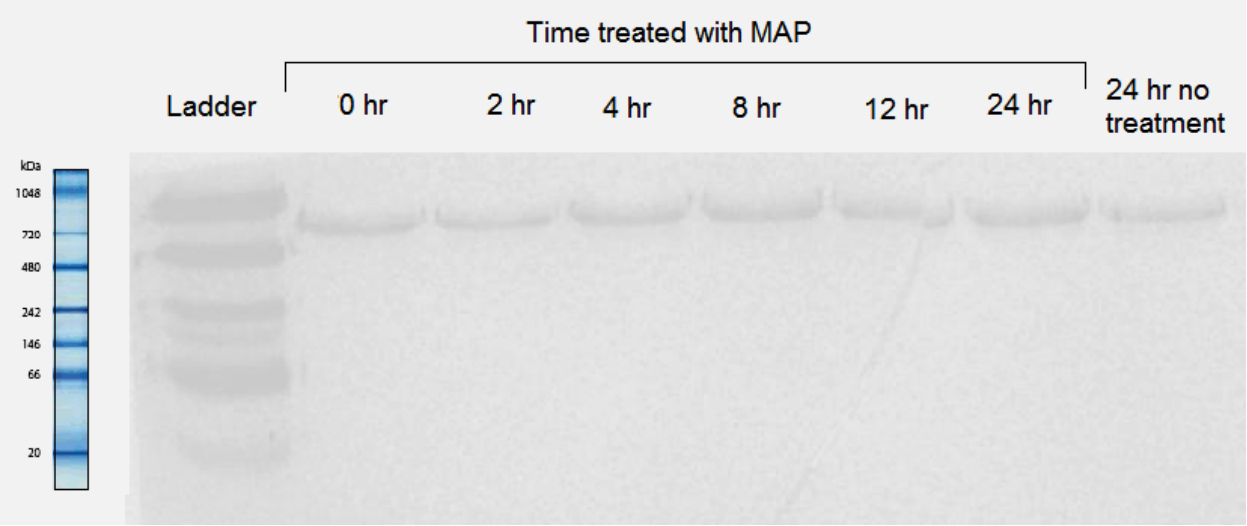

Figure 8 SDS-PAGE for cyclophilin A in HT-29 cells.

0.5 million HT-29 cells were plated, treated with 10 μM MAP-870, and incubated for the amount of time shown above. The supernatant media was then collected, concentrated, and run on the above gel which was stained with Coomassie blue.

Permeability of MAP-870

In addition to examining the mode of cell death caused by MAP-870, the mechanism of MAP-870 cell entry was also investigated. In order to determine the passive membrane permeability of MAP-870 compared to other compounds, a parallel artificial membrane permeability assay (PAMPA) was employed. A PAMPA consists of a thin layer of lipids that mimics a phospholipid bilayer. The ability of a compound to passively diffuse through a PAMPA membrane is indicative of the efficacy of that compound to passively pass through a cell membrane. A PAMPA provides permeability products (P) in cm/s. The experimentally determined permeability products from the PAMPA assay were compared to lipophilicity values (log octanol/water partition coefficient; ClogP) from ChemDraw from which calculated partition coefficients were obtained. The results, shown below in Figure 9 include positive control compounds that display permeability values near that of the calculated partition coefficients and

permeability values previously published. The experimentally determined permeability coefficient for MAP-870 was $0.331 \times 10^{-6} \pm 0.029$ cm/s, similar to 0.269×10^{-6}, the partition coefficent calculated from the ClogP. While there is no consistently obeyed linear relationship between passive diffusion of compounds across cell membranes and their experimentally determined permeability products (P),[70] compounds with permeability products lower than 0.1×10^{-6} cm/s have been reported to have poor oral bioavailability and/or low permeability in CACO-2 cellular permeability assays.[71] Thus compounds with P values near 0.1×10^{-6} cm/s would be expected to have low membrane permeability resulting from passive diffusion. The P value we determined for MAP-870 was near this cut-off, thus raising the question as to whether its pimary mode of cell entry is via passive diffusion or via some other mechanism. According to an

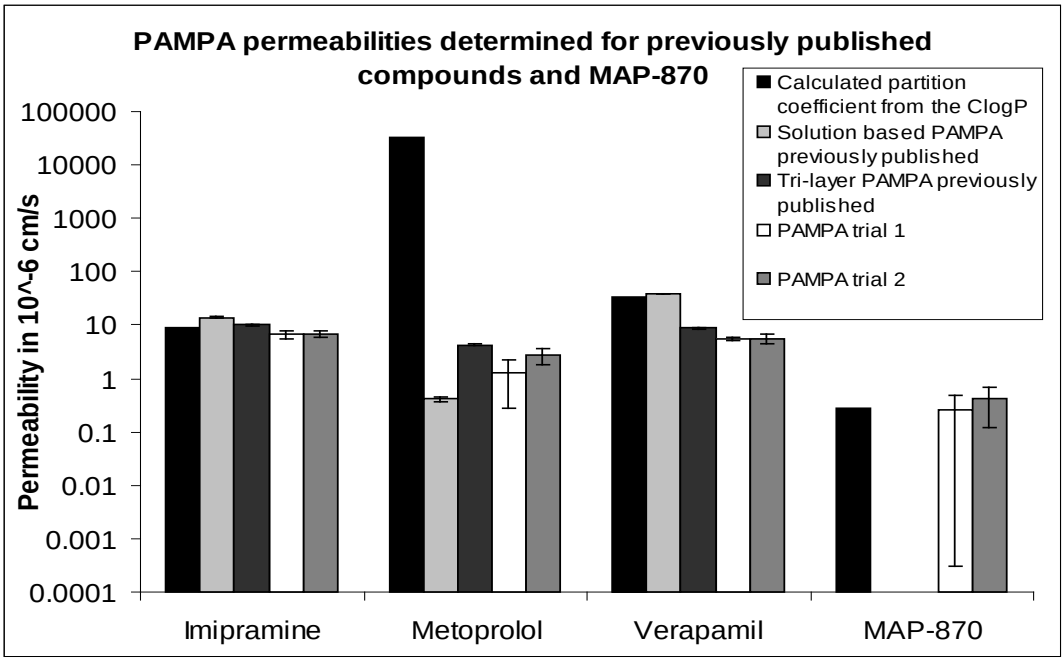

Figure 9 PAMPA permeability compared to ClogP partition coefficient.[72]

The compounds were dissolved in 5% ethanol in PBS and applied to one side of a PAMPA membrane while compound-free 5% ethanol in PBS was added to the other side. After 4 h incubation, the absorbance of the solutions on both sides of the membrane was recorded. Absorbance values were used to calculate the permeability measured.

analysis of a drug database, more than 80% of drugs have a ClogP between -0.4 and 5.6 with an average value of 2.52.[71,73] In addition, the average molecular weight of drugs in the database is 357 ± 174 $gmol^{-1}$. The ClogP and molecular weight of MAP-870 are 6.57 and 670.95, respectively. Thus MAP-870 is outside the average range in both ClogP and molecular weight. According to Ghose et al., outliers like this may be due to the fact that the drug resembles naturally occurring compounds and are transported by active rather than passive diffusion.[73] MAP-870 does have a structural similarity to adenosine and its low GI_{50} could be due to the ubiquity of cellular nucleotide transporters or adenosine A_{2A} receptors which are known to internalize agonists and antagonists via endocytosis.[74]

Confocal images

In order to further examine the mechanism of MAP-870, a biotinylated derivative, JRS-154, was designed. This structure is shown in Figure 13. This molecule was used for confocal microscopy. This was to determine if MAP-870 entered cells and if so where in the cells it was localized. Cells were treated with JRS-154 followed by fixation, permeabilization, and avidin fluorophore conjugate treatment. These cells were visualized using confocal microscopy as shown in Figure 14.

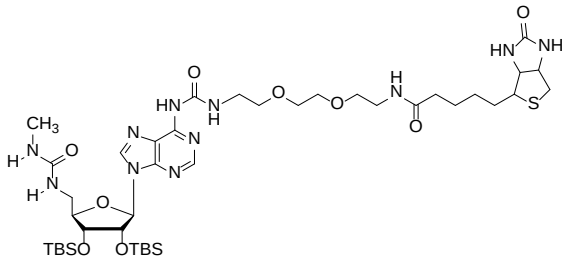

Figure 10 JRS-154, an N6 biotinylated derivative of MAP-870.

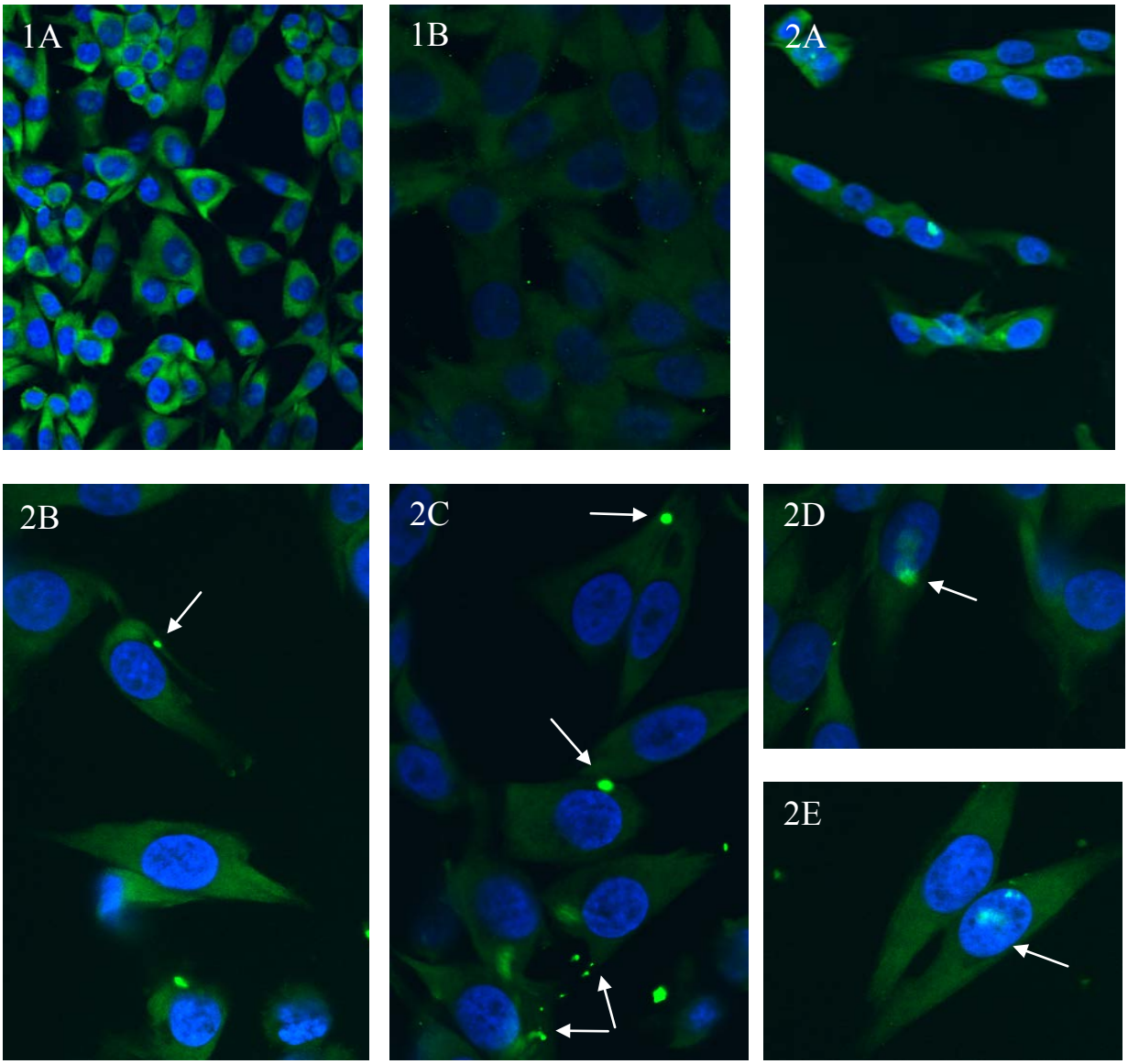

Figure 11 Preliminary confocal images.

All cells stained with both DAPI (blue) and Alexa-fluor488 conjugated avidin (green). The green puncta are due to the Alexa-fluor488 conjugated avidin and are representative of the location of JRS-154. The blue represents the nucleus of the cells stained with DAPI. 1A. DMSO treated cells magnified 20x; 1B. DMSO treated cells magnified 60x; 2A. JRS-154 treated cells magnified 20x; 2B-E JRS-154 treated cells magnified 60x. 2B shows a small puncta in a pseudopod. 2C shows several puncta enclosed in small spaces inside the cell membrane. 2D shows fluorescence entering the nucleus of the cells, and 2E shows fluorescence inside the nucleus.

However, these images are inconclusive. The preliminary data seems to show JRS-154 entering the cells in circular organelles through the pseudopods. The drug then is released and enters the nucleus. However, these puncta could be on the outside of the cells, or they could be a result of the drug binding nonspecifically; more experiments are necessary.

JRS-100

In an effort to optimize MAP-870 activity, MAP-870 derivatives were synthesized using a trial and error based empirical method to determine the SAR of MAP-870 in an attempt to design a more potent and specific molecule. Through this SAR JRS-100, a diphosphate analog, was synthesized (Figure 15) and sent to the NIH NCI for testing.

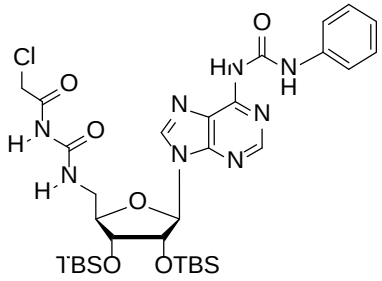

Figure 12 JRS-100, a novel nucleoside with anticancer activity.
JRS-100 is an analog of MAP-870 with similar moieties at the N9, 3′, and 2′ positions, however the 5′ position is a diphosphate analog as opposed to MAP-870 which is a monophosphate analog.

JRS-100 was found to have an average GI_{50} of 0.6 μM and average LC_{50} of 5.6 μM over the cell lines tested, which is significantly more potent than the original MAP-870 compound. The average selectivity index which is calculated by dividing the LC_{50} by the GI_{50} is about 10. This is comparable to a number of currently marketed anticancer agents including chlorambucil, BCNU, methyl-CCNU, fluorodopan, daunorubicin, rifamycin, doxorubicin, and daunorubicin. A selectivity index of 10 is lower than many drugs, however, the most intriguing result discovered

by the NIH was an increased potency against leukemia, with a GI_{50} in one cell line of 16 nM. In order to further test this drug, growth inhibition assays similar to those performed by the NIH were repeated in our lab. For these experiments, two cell lines were used. HT-29 was used because it is the model colon cancer cell line used to test the efficacy of MAP-870, and H23, a lung cancer cell line, was used because it was a cell line in which JRS-100 had a high potency. The GI_{50} of JRS-100 in H23 was determined to be 532 ± 52 nM and in HT-29 to be 272 ± 155 nM, and those found by the NIH NCI to be 756 nM and 330 nM respectively in those cell lines. These results demonstrate that JRS-100 is in fact potent and the similarity of our lab results to the NIH NCI results show that our model is suitable for further mechanistic studies on JRS-100 which are yet to be completed.

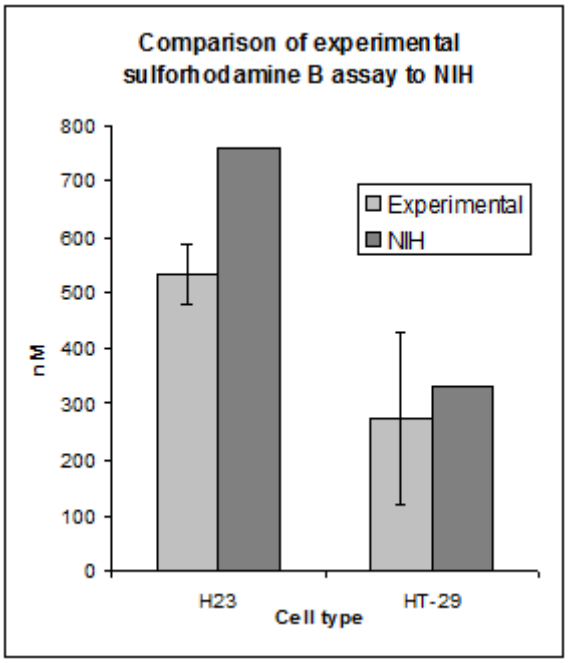

Figure 13 Sulforhodamine B assay determined GI_{50} of JRS-100.

Chapter 4: Discussion

Drug discovery research is less than 150 years old. It began with the theory that the cells of microorganisms and cancers had different chemoreceptors than the host, so drugs could target these chemoreceptors and inhibit them specifically.[75] The process of modern drug design is shown in Scheme 2. In the past, the idea-phase of drug discovery began with herbs that induced reactions that were useful for medications. The active compounds of these herbs were purified, and derivatives were made to increase potency and specificity thereby reducing side effects. Often the structure and mechanism of the drug was discovered much later.

Today however, with our knowledge of biological systems including genomes and proteomes, potential targets can be identified and drugs then produced to act on them. This process is referred to as rational drug design. In rational drug design, biologists or biochemists discover a pathway or protein that would hypothetically make a good drug target. Then chemists find potential drugs using massive screening techniques. These techniques involve high-throughput screening for target inhibition using libraries of molecules, either *in vitro* or *in silico*. These high-throughput screening techniques have resulted in millions more data points than previous methods of drug discovery; however, there has not yet been an accompanying increase in pharmaceutical industry productivity.[75] This may be due to the fact that this new method of drug discovery is only recently being optimized and still has shortcomings. One such shortcoming is non-specific binding, where a molecule found to bind to a target protein also binds to other proteins making it an ineffective drug. Another shortcoming includes the testing of drugs *in vitro* and *in silico* which cannot yet match the complexity of in vivo systems.

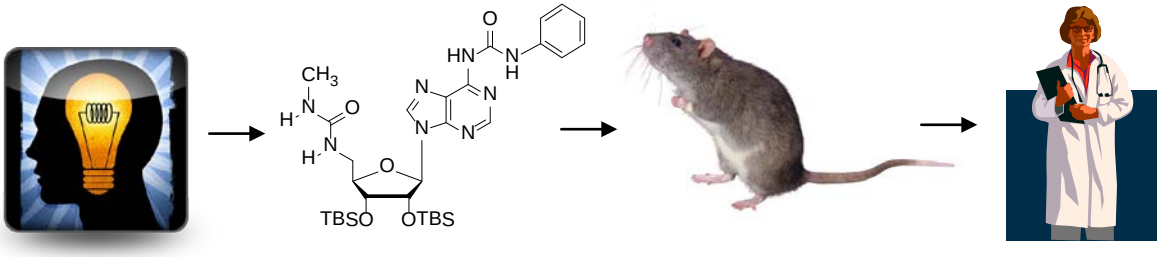

Scheme 2 Drug discovery process modified from Lombardino and Lowe.[76]

An example of these setbacks can be seen when this approach was used to design a drug to inhibit HIV integrase. The screening process was completed *in silico*, and MAP-870 was the result.[77] MAP-870 was unsuccessful at its intended purpose; however, it was found to have anticancer activity. As mentioned above, NDs that interfere with DNA are used to treat both viruses and cancer and often have very similar mechanisms; so although unanticipated, this result is not unique. Several NDs that are expected to act on one disease have been found to act on another.[20]

In the study of the anticancer activity of MAP-870, it was discovered that MAP-870 (sans TBS groups) binds to several protein kinases, but most specifically to bone morphogenetic protein receptor 1B (BMPR1B) with a K_d of 11.5 ± 0.7 μM.[19] BMPR1B is a receptor of the TGFβ superfamily. The working model of the mechanism of MAP-870 is shown in Scheme 3. It is hypothesized that MAP-870 enters cells via ND receptors such as purine P2 receptors or adenosine A_{2A} receptors which undergo agonist-mediated endocytosis. This endocytosis occurs through clathrin-coated pits causing the receptor and agonist to be localized in early endosomes.[78] If the resultant endosomes combine with lysosomes, then a concomitant decrease in pH could destabilize the oxygen-silicon bond in MAP-870 thereby breaking the bond and detaching the TBS groups.

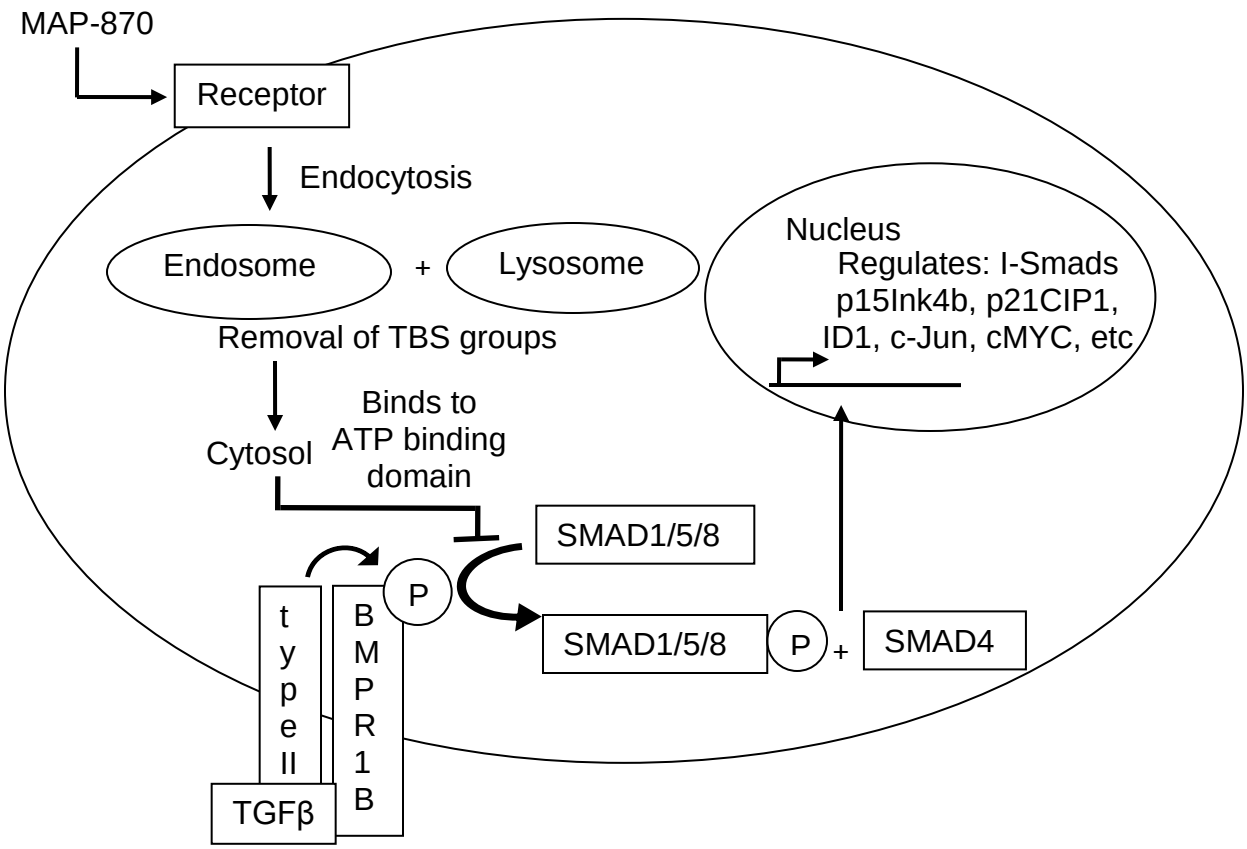

Scheme 3 Working model for the MAP-870 mechanism.

Type II refers to a type II TGFβ receptor. ID1, DNA-binding protein inhibitor, is necessary for cell survival. Cells lacking ID1 undergo apoptosis.[79–81]

The TBS-free MAP-870 binds with good affinity (Kd = 11.5 ± 0.7 μM) to bone morphogenetic protein receptor type-1B (BMPR1B), a transmembrane serine/threonine kinase.[25,82] MAP-870 binds to the ATP binding site of BMPR1B, inhibiting its enzymatic activity. BMPRIB is phosphorylated by a type II receptor bound to a TGFβ ligand. This phosphorylation causes FKBP12, an inhibitory protein, to dissociate from BMPR1B thereby allowing SMADs to bind.[80] These receptor regulated SMADs, SMADs 1, 5, and 8, are phosphorylated by BMPR1B. This step is thought to be inhibited by MAP-870. Phosphorylated SMADs 1, 5, and 8 then dissociate from cytoplasmic retention proteins revealing nuclear import signals, and are transported into the nucleus. These receptor-regulated SMADs then bind to

SMAD4, which has a higher affinity for DNA, and together the SMADs act as transcription factors. SMADs affect the transcription of many proteins including p15INK4b, p21CIP1, c-MYC, and ID. ID1 is activated by this pathway and normally prevents type I PCD. We hypothesized that MAP-870 would cause this type of cell death because without phosphorylated SMAD 1, 5, and 8, ID1 is not activated, and type I PCD would therefore result.

The pathway of the TGFβ super family is not yet firmly understood. Drugs that target and inhibit the TGFβ pathway have been designed. However, this pathway can either suppress or promote tumors depending on the type of tumor and the stage in progression.[80] Generally, in early stages of tumorigenesis TGFβ acts as a tumor suppressor, but as the tumor progresses TGFβ plays a vital part in epithelial-mesenchymal transition (EMT), a harbinger of metastasis.[80,81] Then, once the cancer has become malignant, TGFβ acts a tumor promoter.[81] That is why in some cancers SMAD4 is mutated or completely lost to counteract the tumor suppressing characteristics of the TGFβ pathway. However, in other cancers only the tumor suppressing arm of the TGFβ pathway is inhibited so the cells can take advantage of the EMT-inducing and tumor promoting arm of the pathway.[80]

The complexity of this pathway may make it a promising target for treatment and aid in making MAP-870 specific, but it also means that the results of targeting this pathway are at present unpredictable. This could explain why the results discussed in this thesis were different than the results that were expected. However, the addition of microarray analysis of specific tumors to classify their response to TGFβ, coupled with a better understanding of the mechanism of MAP-870 could lead ultimately to the development of specific, unique cancer treatments. In addition, further study of MAP-870 may be a powerful tool for better understanding the TGFβ pathway.[83]

Two other ATP competitive compounds, SB-505124 and SB-431542, have been shown to inhibit the TGFβ pathway.[81] These drugs inhibit other type I receptors namely ALK4, ALK5, and ALK7.[83,84] Our compound is a potential TGFβ type I receptor inhibitor inhibiting BMPR1B (also known as ALK6). If MAP-870 does act by inhibiting BMPR1B, it would exemplify a novel approach at inhibiting the TGFβ pathway. TGFβ plays a prominent part in cancer and metastasis, therefore MAP-870 definitely merits further examination.

In order to study the mechanism of MAP-870, several experiments were completed including trypan blue cell quantification, sulforhodamine B assays, Caspase-Glo3/7 assays, DNA fragmentation detection, cyclophilin A release detection, PAMPAs, confocal imaging, and flow cytometry of cell cycle, PI incorporation, and PS externalization.

Sulforhodamine B assays show that MAP-870 does indeed cause growth inhibition and cell death in the model tested. The first step working model above (Scheme 3) is supported by PAMPAs that show that MAP-870 does not appear to enter the cell via passive diffusion, and probably enters the cell through either active transporters or endocytosed receptors. The working model led us to believe that MAP-870 treatment would result in the induction of type I PCD; however, flow cytometry showed that MAP-870 does not appear to cause cell cycle arrest or externalization of PS. In addition, Caspase-Glo3/7 assays demonstrated that MAP-870 does not appear to cause caspase activation. Combining this data, it appears that MAP-870 causes cell death without PS exposure or caspase activation (Scheme 3). However, the complexity of the TGFβ pathway could easily render unpredictable results from drugs that inhibit it. The results discussed here may help determine if the TGFβ pathway is being affected and if so what arm of the pathway and thereby what cancers MAP-870 would be effective at treating.

Using the working model mentioned above, it was hypothesized that MAP-870 causes ID1 inhibition resulting in type I PCD. However, type I PCD almost always occurs with caspase activation. In addition, during almost all types of cell death mechanisms, with few exceptions, the dying cell causes PS to be externalized to the outer leaflet.[37,85] PS exposure is almost always characteristic of type I PCD.[36] Above experiments showed that when treated with MAP-870, HT-29 cells did not demonstrate activation of caspases or externalization of PS. Confocal images also did not show nuclear fragmentation, as is characteristic of apoptosis. However, the lack of evidence of PS externalization does not necessarily exclude type I PCD as the mechanism of cell death. Some weaknesses associated with the annexin V assay used to determine PS exposure include decreased sensitivity in cultures with a low level of apoptosis or with asynchronous death.[39,86] In addition, it is also known that type I PCD under low ATP conditions occurs without PS externalization.[87] These limitations to the annexin V assay make it impossible to unambiguously conclude that MAP-870 does not induce apoptosis, although it does seem unlikely in the light of the results obtained in our assays.

Caspase-independent type I PCD was also considered as a possibility because PS exposure is usually caspase dependent. However, PS exposure has been found in caspase-independent apoptosis.[35,88] Most notably, the caspase-independent apoptosis which is triggered by apoptosis inducing factor (AIF) causes phosphatidylserine externalization.[87,89] The above-mentioned weaknesses in the PS exposure assay mean that caspase-independent type I PCD could possibly be occurring. However, caspase-independent cell death is usually characterized in cells, that when treated with a chemical agent, undergo cell death that in all respects looks like apoptosis. The apoptosis of these cells includes caspase activation, and caspase-independence is determined by either treating the cells with caspase inhibitors or genetically inactivating the

caspases of the cells.[51] If the treated cells still die, in spite of the caspase inhibition, the cell death mechanism is described as caspase-independent cell death. However, it is argued that these cells only share the fact that they cannot be protected by caspase inhibition, and they may not share a uniform mechanism.[51] If there is a shared mechanism, it is probably a result of the cytotoxic agents causing mitochondrial outer membrane permeabilization (MOMP) which causes caspase activation and is toxic to cells regardless of caspase activation. The inherent toxicity of MOMP makes it so cells treated with caspase inhibitors are not protected.[51] In conclusion, it is improbable that MAP-870 causes caspase-independent cell death because MAP-870 does not cause caspase-activation or PS exposure.

Next, type II PCD was considered, because PS externalization is usually characteristic of apoptosis, and autophagy could alter PS externalization.[28,90] However, PS externalization has been found in some cases of autophagic cell death, and according to one author PS is externalized during autophagy as it is in apoptosis.[44,47,91] Some even claim autophagy is required for PS externalization in conjunction with apoptosis.[92]

Type III PCD was also considered, but necrosis generally includes PS exposure and cell membrane permeabilization neither of which was observed in our assays. That makes necrosis unlikely for the mechanism of cell death exerted by MAP-870.

Mitotic cell death, like apoptosis, occurs through the activation of caspases. Therefore, mitotic cell death, despite being utilized in some ND drug pathways, is also not a likely candidate for the mechanism of cell death for MAP-870.[93]

In a search to determine the type of programmed cell death (PCD) induced by MAP-870, mechanisms of PCD which don't follow classical rules were examined. Those mentioned in the introduction are not very well defined, but could possibly be occurring in this model. One

example of cell death without PS exposure or caspase activation is induced in "substance P" treated cultures of hippocampal, cortical, and striatal neurons.[94] These treated cells exhibit caspase-independent cell death without membrane blebbing, nuclear fragmentation, or PS externalization.[94]

Other exceptions to the rule that PS is externalized during cell death include patients with Scott syndrome, whose cells cannot externalize PS upon exposure to Ca^{2+}. These patients have a defect in blood coagulation cause by PS externalization defects because PS is externalized in platelets when they are activated. PS is used as a binding site for plasma complexes, and patients without it experience excessive bleeding.

Other examples occur in vitro. In fact, PS externalization has been found to be very cell-line dependent.[32] For example, one research group found no increase in PS externalization in HL-60, P39, and Raji cells upon apoptotic stimuli.[36] In addition, apoptotic Raji cells that are transfected with the scramblase gene externalize PS in response to Ca^{2+} but not in response to apoptotic stimuli.[38] The above experiment included a variety of apoptotic signals, however all cells under all apoptotic treatments showed an increase in caspase activity.[36]

In conclusion, at this point in time the cell death seen in HT-29 cells when treated with MAP-870 cannot be categorized unambiguously. A recent publication by Melino et al. has suggested that due to the plethora of complex mechanisms causing cell death, scientists should steer away from rigid classifications of cell death and instead focus on understanding the (often times) unique biochemical pathways behind cell processing in each individual case.[47] The complexity of the proposed mechanism of action, through the TGFβ pathway, could understandably cause a complex mechanism of cell death that may not fit into simple categorizations.

To summarize, the biochemical pathway leading to cell death caused by MAP-870 is complex and requires further study. According to sulforhodamine B assays, MAP-870 causes a decrease in biomass of treated HT-29 cells. MAP-870 also causes an increase in cellular debris measured by flow cytometry. This same flow cytometry experiment showed that MAP-870 does not appear to cause cell cycle arrest in HT-29 cells. In addition, it appears that this mode of cell death is caspase-independent in HT-29 cells according to the results of our Caspase-Glo3/7 assays. Additional flow cytometry experiments show that MAP-870 does not appear to cause membrane permeabilization or PS externalization. It also appears that MAP-870 does not enter cancer cells via passive diffusion. From confocal spectroscopy, it appears preliminarily that MAP-870 is taken up by cells, often through pseudopodes. From these images it also appears that MAP-870 is entering the nucleus, so perhaps it is there that it exerts its effects.

The mechanism of MAP-870 on cancer cells must be further studied to elucidate its mechanism of action. Further confocal studies are needed at several time points to track MAP-870 as it affects cancer cells. These experiments could include cells treated with JRS-154 at different time points and cells treated with a control molecule that would not be able to enter the cells. Also, more detailed Z-stacked scans could show three dimensional detail about where MAP-870 is localized. In addition, a MAP-870 fluorophore conjugate chould be designed so that the cells can be co-stained with lysotracker. Lysotracker is a stain that only fluoresces at a low pH, so it selectivly stains lysosomes. Using this stain, it could be determined if the puncta inside the cell are in fact MAP-870 inside lysosomes.

In addition, it would be advisable to do more protein studies. An immunoblot would be useful to see if BMPR1B binds *in vivo* to JRS-154 (MAP-870 attached to biotin) and an avidin

fluorophore. Positive results could further demonstrate the role of MAP-870 in the TGFβ pathway. In addition, further binding studies may also be of use.

Finally, other MAP-870 analogs need to be further studied including JRS-100. In addition, MAP-870 is probably actively transported into cells and does not seem to enter cells by diffusion, therefore new MAP-870 analogs that are more water soluble could enhance activity. These drugs would be easier to examine, and would have more reliable concentrations, and could have potentially higher activity.

WORK CITED

(1) Watson, J. D.; Crick, F. H. C. *Nature* **1953**, *171*, 737–738.
(2) *Purinethol*; Drugs@FDA; US Food and Drug Administration, 1953.
(3) Sahasranaman, S.; Howard, D.; Roy, S. *Eur. J. Clin. Pharmacol.* **2008**, *64*, 753–767.
(4) Kaye, S. B. *Brit. J. Cancer* **1998**, *78*, 1–7.
(5) *US Food and Drug Administration (FDA), Drugs@FDA*; US Food and Drug Administration.
(6) Li, J. *Modern drug synthesis*; Wiley: Hoboken N.J., 2010.
(7) Sams-Dodd, F. *Drug Discov. Today* **2006**, *11*, 465–472.
(8) Hatse, S.; De Clercq, E.; Balzarini, J. *Biochem. Pharmacol.* **1999**, *58*, 539–555.
(9) Salser, J. S.; Hutchison, D. J.; Balis, M. E. *J. Biol. Chem.* **1960**, *235*, 429 –432.
(10) Petit, E.; Langouet, S.; Akhdar, H.; Nicolas-Nicolaz, C.; Guillouzo, A.; Morel, F. *Toxicol. In Vitro* **2008**, *22*, 632–642.
(11) Cara, C. J.; Pena, A. S.; Sans, M.; Rodrigo, L.; Guerrero-Esteo, M.; Hinojosa, J.; García-Paredes, J.; Guijarro, L. G. *Med. Sci. Monit.* **2004**, *10*, RA247–254.
(12) Inamochi, H.; Higashigawa, M.; Shimono, Y.; Nagata, T.; Cao, D. C.; Mao, X. Y.; M'soka, T.; Hori, H.; Kawasaki, H.; Sakurai, M. *J. Exp. Clin. Cancer Res* **1999**, *18*, 417–424.
(13) Månsson, E.; Spasokoukotskaja, T.; Sällström, J.; Eriksson, S.; Albertioni, F. *Cancer Res.* **1999**, *59*, 5956 –5963.
(14) Fabianowska-Majewska, K.; Wyczechowska, D. *Acta. Pol. Pharm.* **1996**, *53*, 231–239.
(15) Lotfi, K.; Mansson, E.; Chandra, J.; Wang, Y.; Xu, D.; Knaust, E.; Spasokoukotskaja, T.; Liliemark, E.; Eriksson, S.; Albertioni, F. *Brit. J. Haematol.* **2001**, *113*, 339–346.
(16) Albertioni, F.; Lindemalm, S.; Eriksson, S.; Juliusson, G.; Liliemark, J. *Adv. Exp. Med. Biol.* **1998**, *431*, 693–697.
(17) Parker, W. B.; Shaddix, S. C.; Chang, C.-H.; White, E. L.; Rose, L. M.; Brockman, R. W.; Shortnacy, A. T.; Montgomery, J. A.; Secrist, J. A.; Bennett, L. L. *Cancer Res.* **1991**, *51*, 2386–2394.
(18) Leoni, L. M.; Chao, Q.; Cottam, H. B.; Genini, D.; Rosenbach, M.; Carrera, C. J.; Budihardjo, I.; Wang, X.; Carson, D. A. *Proc. Natl. Acad. Sci.* **1998**, *95*, 9567–9571.
(19) Shelton, J. R.; Cutler, C. E.; Oliveira, M.; Balzarini, J.; Peterson, M. A. *Bioorg. Med. Chem. Lett* **2012**, *20*, 1008–1019.
(20) Broder, S. *Antivir. Res.* **2010**, *85*, 1–18.
(21) Bains, W.; Tacke, R. *Curr. Opin. Drug Discov. Devel.* **2003**, *6*, 526–543.
(22) Peterson, M. A.; Oliveira, M.; Christiansen, M. A.; Cutler, C. E. *Bioorgan. Med. Chem.* **2009**, *19*, 6775–6779.
(23) Methodology http://dtp.nci.nih.gov/docs/compare/compare_methodology.html (accessed Dec 26, 2011).
(24) Screening Services – NCI-60 DTP Human Tumor Cell Line Screen http://dtp.nci.nih.gov/branches/btb/ivclsp.html (accessed Aug 8, 2012).
(25) Shelton, J. R.; Burt, S. R.; Peterson, M. A. *Bioorg. Med. Chem. Lett.* **2011**, *21*, 1484–1487.
(26) Gunnarsdottir, S.; Elfarra, A. A. *Drug Metab. Dispos.* **2004**, *32*, 321–327.
(27) Hanahan, D.; Weinberg, R. A. *Cell* **2011**, *144*, 646–674.
(28) Bursch, W.; Ellinger, A.; Gerner, C.; FröHwein, U.; Schulte-Hermann, R. *Ann. N. Y. Acad. Sci.* **2006**, *926*, 1–12.

(29) Kroemer, G.; Galluzzi, L.; Vandenabeele, P.; Abrams, J.; Alnemri, E. S.; Baehrecke, E. H.; Blagosklonny, M. V.; El-Deiry, W. S.; Golstein, P.; Green, D. R.; Hengartner, M.; Knight, R. A.; Kumar, S.; Lipton, S. A.; Malorni, W.; Nuñez, G.; Peter, M. E.; Tschopp, J.; Yuan, J.; Piacentini, M.; Zhivotovsky, B.; Melino, G. *Cell Death Differ.* **2008**, *16*, 3–11.
(30) Zong, W.-X. *Genes & Development* **2004**, *18*, 1272–1282.
(31) Liu, T.; Brouha, B.; Grossman, D. *Oncogene* **2004**, *23*, 39–48.
(32) Utsugi, T.; Schroit, A. J.; Connor, J.; Bucana, C. D.; Fidler, I. J. *Cancer Res.* **1991**, *51*, 3062–3066.
(33) Martin, S. J.; Reutelingsperger, C. P.; McGahon, A. J.; Rader, J. A.; van Schie, R. C.; LaFace, D. M.; Green, D. R. *J. Exp. Med.* **1995**, *182*, 1545–1556.
(34) Koopman, G.; Reutelingsperger, C.; Kuijten, G.; Keehnen, R.; Pals, S.; van Oers, M. *Blood* **1994**, *84*, 1415–1420.
(35) Ferraro-Peyret, C.; Quemeneur, L.; Flacher, M.; Revillard, J.-P.; Genestier, L. *The J. Immun.* **2002**, *169*, 4805–4810.
(36) Fadeel, B.; Gleiss, B.; Högstrand, K.; Chandra, J.; Wiedmer, T.; Sims, P. J.; Henter, J.-I.; Orrenius, S.; Samali, A. *Biochem. Biophys. Res. Commun.* **1999**, *266*, 504–511.
(37) Balasubramanian, K.; Mirnikjoo, B.; Schroit, A. J. *J. Biol. Chem.* **2007**, *282*, 18357–18364.
(38) Balasubramanian, K.; Schroit, A. J. *Ann. Rev. Phys.* **2003**, *65*, 701–734.
(39) Kunapuli, S.; Rosanio, S.; Schwarz, E. R. *J. Cardiac Failure* **2006**, *12*, 381–391.
(40) Coates, J. M.; Galante, J. M.; Bold, R. J. *J. Surgical Res.* **2010**, *164*, 301–308.
(41) Paglin, S.; Hollister, T.; Delohery, T.; Hackett, N.; McMahill, M.; Sphicas, E.; Domingo, D.; Yahalom, J. *J. Cancer Res.* **2001**, *61*, 439 –444.
(42) Kanzawa, T.; Kondo, Y.; Ito, H.; Kondo, S.; Germano, I. *Cancer Res.* **2003**, *63*, 2103 – 2108.
(43) Shao, Y.; Gao, Z.; Marks, P. A.; Jiang, X. *Proc. Natl. Acad. Sci.* **2004**, *101*, 18030–18035.
(44) Amaravadi, R. K.; Thompson, C. B. *Clin. Can. Res.* **2007**, *13*, 7271–7279.
(45) Christofferson, D. E.; Yuan, J. *Cell Death Differ.* **2010**, *17*, 1942–1943.
(46) Goodman, L. *Journal of Clinical Investigation* **2004**, *113*, 1662–1662.
(47) Melino, G.; Knight, R. A.; Nicotera, P. *Cell Death Differ.* **2005**, *12*, 1457–1462.
(48) Gilmore, A. P. *Cell Death Differ.* **2005**, *12*, 1473–1477.
(49) Coleman, M. P.; Freeman, M. R. *Ann. Rev. Neurosci.* **2010**, *33*, 245–267.
(50) Jaiswal, M.; Zech, W.-D.; Goos, M.; Leutbecher, C.; Ferri, A.; Zippelius, A.; Carrì, M.; Nau, R.; Keller, B. U. *BMC Neurosci.* **2009**, *10*, 64.
(51) Kroemer, G.; Martin, S. J. *Nature Med.* **2005**, *11*, 725–730.
(52) Ishitsuka, K. *Blood* **2005**, *106*, 1794–1800.
(53) Panka, D. J. *Cancer Res.* **2006**, *66*, 1611–1619.
(54) Miguet, C.; Monier, S.; Bettaieb, A.; Athias, A.; Besséde, G.; Laubriet, A.; Lemaire, S.; Néel, D.; Gambert, P.; Lizard, G. *Cell Death Differ.* **2001**, *8*, 83–99.
(55) Urick, M. E.; Chung, E. J.; Shield, W. P.; Gerber, N.; White, A.; Sowers, A.; Thetford, A.; Camphausen, K.; Mitchell, J.; Citrin, D. E. *Clin. Can. Res.* **2011**, *17*, 5038–5047.
(56) Sperandio, S. *Proc. Natl. Acad. Sci.* **2000**, *97*, 14376–14381.
(57) Sperandio, S.; Poksay, K.; de Belle, I.; Lafuente, M. J.; Liu, B.; Nasir, J.; Bredesen, D. E. *Cell Death Differ.* **2004**, *11*, 1066–1075.
(58) American Chemical Society Cancer Facts & Figures **2011**.
(59) Freshney, R. *Culture of animal cells : a manual of basic technique and specialized applications*; 6th ed.; Wiley-Blackwell: Hoboken N.J., 2010.

(60) Pozarowski, P.; Grabarek, J.; Darzynkiewicz, Z. *Curr. Protoc. Cell Biol.* **2004**, *Chapter 18*, Unit 18.8.
(61) Laemmli, U. K. *Nature* **1970**, *227*, 680–686.
(62) Taylor, R. M. FASP http://openwetware.org/wiki/Prince:FASP (accessed Dec 28, 2011).
(63) Voigt, W. *Methods Mol. Med.* **2005**, *110*, 39–48.
(64) Groschel, B.; Bushman, F. *J. Virol.* **2005**, *79*, 5695–5704.
(65) Tsao, Y. P.; D'Arpa, P.; Liu, L. F. *Cancer Res.* **1992**, *52*, 1823–1829.
(66) Robak, T.; Lech-Maranda, E.; Korycka, A.; Robak, E. *Curr. Med. Chem.* **2006**, 3165–3189.
(67) Pozarowski, P.; Grabarek, J.; Darzynkiewicz, Z. In *Current Protocols in Cytometry*; Robinson, J. P.; Darzynkiewicz, Z.; Dobrucki, J.; Hyun, W. C.; Nolan, J. P.; Orfao, A.; Rabinovitch, P. S., Eds.; John Wiley & Sons, Inc.: Hoboken, NJ, USA, 2003.
(68) Vermes, I.; Haanen, C.; Steffens-Nakken, H.; Reutellingsperger, C. *J. Immunol. Methods* **1995**, *184*, 39–51.
(69) *BD Biosciences Support - Protocols - Apoptosis - Cell Death Induced by Camptothecin*.
(70) Summerfield, S. G.; Read, K.; Begley, D. J.; Obradovic, T.; Hidalgo, I. J.; Coggon, S.; Lewis, A. V.; Porter, R. A.; Jeffrey, P. *Journal of Pharmacology and Experimental Therapeutics* **2007**, *322*, 205–213.
(71) Artursson, P.; Karlsson, J. *Biochem. Biophys. Res. Commun.* **1991**, *175*, 880–885.
(72) Chen, X.; Murawski, A.; Patel, K.; Crespi, C. L.; Balimane, P. V. *Pharm. Res.* **2008**, *25*, 1511–1520.
(73) Ghose, A. K.; Viswanadhan, V. N.; Wendoloski, J. J. *Journal of Combinatorial Chemistry* **1999**, *1*, 55–68.
(74) Thorn, J. A.; Jarvis, S. M. *Gen. Pharmacol.* **1996**, *27*, 613–620.
(75) Drews, J. *Science* **2000**, *287*, 1960–1964.
(76) Lombardino, J. G.; Lowe, J. A. *Nat. Rev. Drug Discov.* **2004**, *3*, 853–862.
(77) Peterson, M. A.; Ke, P.; Shi, H.; Jones, C.; McDougall, B. R.; Robinson, W. E. *Nucleos. Nucleot. Nuc.* **2007**, *26*, 499–519.
(78) Brand, F.; Klutz, A. M.; Jacobson, K. A.; Fredholm, B. B.; Schulte, G. *Eur. J. Pharmacol.* **2008**, *590*, 36–42.
(79) Ying, Q.-L.; Nichols, J.; Chambers, I.; Smith, A. *Cell* **2003**, *115*, 281–292.
(80) Padua, D.; Massagué, J. *Cell Res.* **2009**, *19*, 89–102.
(81) Jeon, H.-S.; Jen, J. *J. Thorac. Oncol.* **2010**, *5*, 417–419.
(82) Souza, C. *J. Endocrin.* **2001**, *169*, R1–R6.
(83) DaCosta Byfield, S. *Molec. Pharmacol.* **2004**, *65*, 744–752.
(84) Inman, G. J.; Nicolas, F. J.; Callahan, J. F.; Harling, J. D.; Gaster, L. M.; Reith, A. D.; Laping, N. J.; Hill, C. S. *Molec. Pharmacol.* **2002**, *62*, 65–74.
(85) Elliott, J. I.; Surprenant, A.; Marelli-Berg, F. M.; Cooper, J. C.; Cassady-Cain, R. L.; Wooding, C.; Linton, K.; Alexander, D. R.; Higgins, C. F. *Nature Cell Biol.* **2005**, *7*, 808–816.
(86) Gottlieb, R. A.; Kitsis, R. N. *Nat. Med.* **2001**, *7*, 1277–1278.
(87) Bras, M.; Queenan, B.; Susin, S. A. *Biochemistry (Moscow)* **2005**, *70*, 231–239.
(88) Carmody, R. J.; Cotter, T. G. *Cell Death Differ.* **2000**, *7*, 282–291.
(89) Candé, C.; Cecconi, F.; Dessen, P.; Kroemer, G. *J. Cell Sci.* **2002**, *115*, 4727 –4734.
(90) Kroemer, G.; Levine, B. *Nature Rev. Molec. Cell Biol.* **2008**, *9*, 1004–1010.
(91) Madden, D. T.; Egger, L.; Bredesen, D. E. *Autophagy* **2007**, *3*, 519–522.
(92) Mizushima, N. *Genes & Development* **2007**, *21*, 2861–2873.

(93) Castedo, M.; Perfettini, J.-L.; Roumier, T.; Andreau, K.; Medema, R.; Kroemer, G. *Oncogene* **2004**, *23*, 2825–2837.
(94) Castro-Obregón, S.; Del Rio, G.; Chen, S. F.; Swanson, R. A.; Frankowski, H.; Rao, R. V.; Stoka, V.; Vesce, S.; Nicholls, D. G.; Bredesen, D. E. *Cell Death Differ.* **2002**, *9*, 807–817.

APPENDIX A

Raw data for a sample cell cycle arrest flow cytometry in HT-29. HT-29 cells were plated and incubated for 24 h after which they were treated and incubated for an additional 48 h. Cell fixation and propidium iodide staining was performed and 10,000 cell samples were analyzed by flow cytometry. The graph in the upper left shows forward scatter (x-axis) and side scatter (y-axis) for the given cells. The parent population was selected from this graph as the counts most likely to be whole cells. The graph on the upper right shows the width of the PI peak (x-axis) plotted against the area of the PI peak (y-axis) of the parent population. The data below that was processed using ModFit LT, and the numbers in blue to the right were used to generate Figure 5. In said numbers, Dip stands for diploid. A. Untreated cells; B. Vehicle control (0.1% DMSO) treated cells; C. 10 μM camptothecin treated cells; D. 25 μM MAP-870 treated cells; E. 10 μM MAP-870 treated cells; F. 5 μM MAP-870 treated cells.

A.

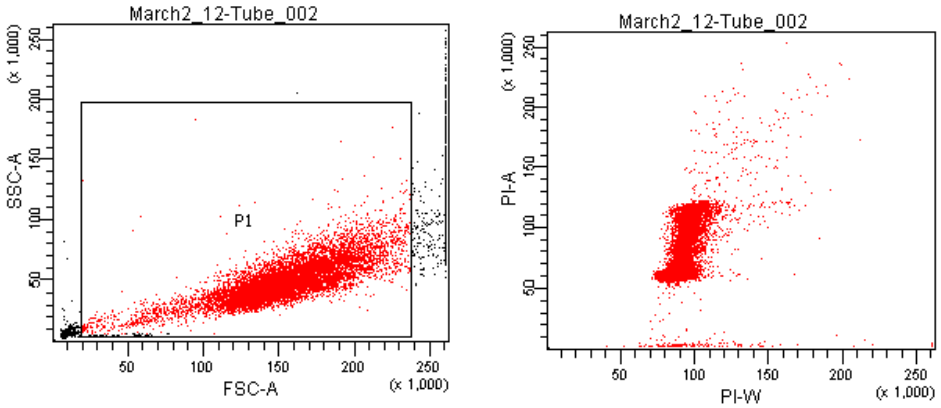

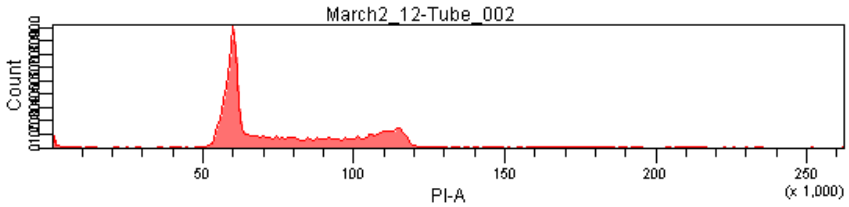

Tube: Tube_002

Population	#Events	%Parent	%Total
All Events	10,000	####	100.0
P1	8,845	88.4	88.4

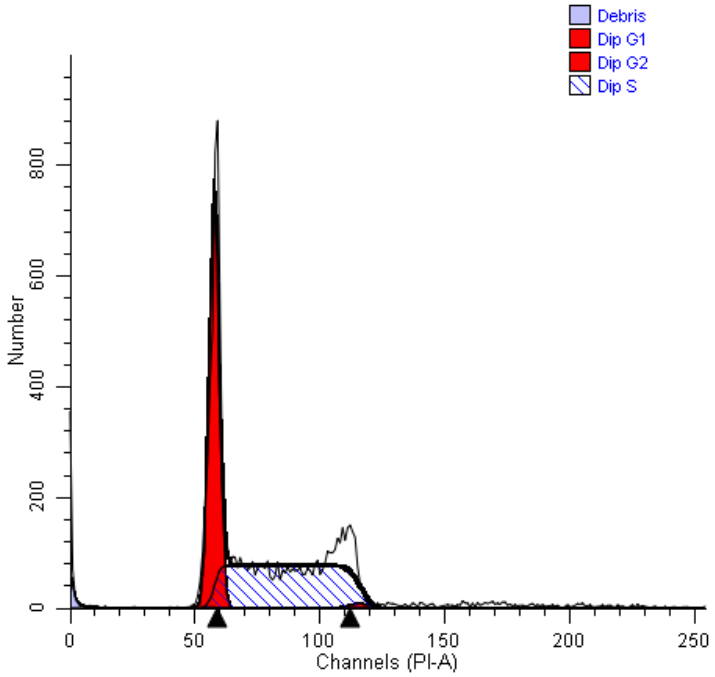

File analyzed: March2_12_Tube_002.fcs
Date analyzed: 2-Mar-2012
Model: 1Dn0n_DSD
Analysis type: Manual analysis

Ploidy Mode: First cycle is diploid

Diploid: 100.00 %
Dip G1: 44.43 % at 57.93
Dip G2: 0.98 % at 115.86
Dip S: 54.59 % G2/G1: 2.00
%CV: 3.40

Total S-Phase: 54.59 %
Total B.A.D.: 0.24 % no aggs

Debris: 2.40 %
Aggregates: 0.00 %
Modeled events: 8411
All cycle events: 8209
Cycle events per channel: 139
RCS: 5.431

B.

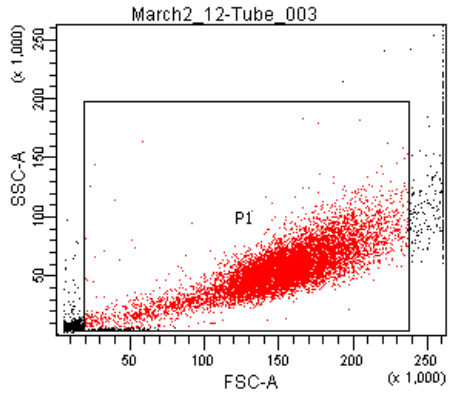

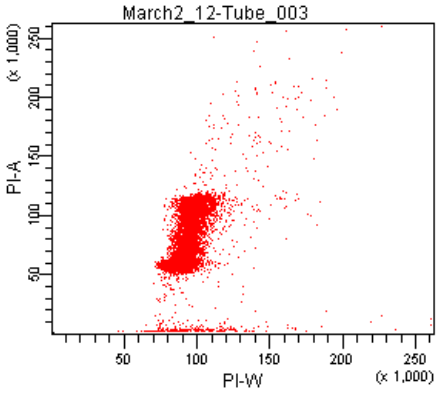

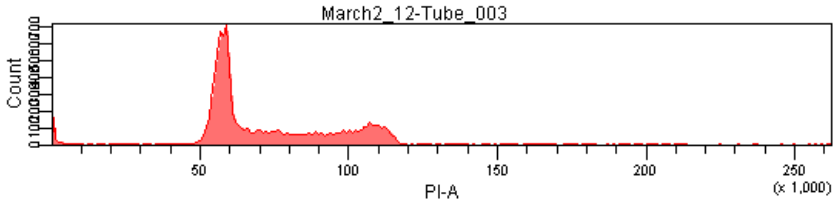

Tube: Tube_003

Population	#Events	%Parent	%Total
All Events	10,000	####	100.0
P1	8,985	89.8	89.8

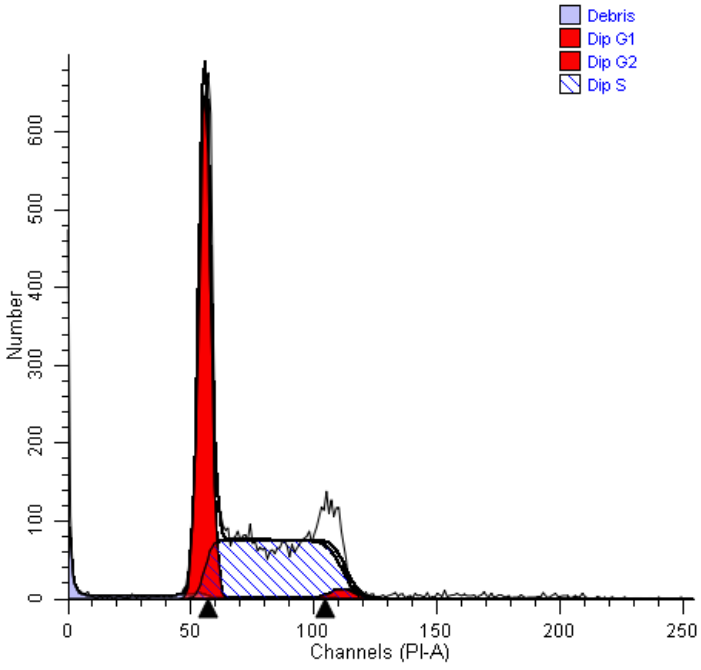

File analyzed: March2_12_Tube_003.fcs
Date analyzed: 2-Mar-2012
Model: 1Dn0n_DSD
Analysis type: Manual analysis

Ploidy Mode: First cycle is diploid

Diploid: 100.00 %
Dip G1: 47.83 % at 55.77
Dip G2: 1.78 % at 111.55
Dip S: 50.39 % G2/G1: 2.00
%CV: 4.37

Total S-Phase: 50.39 %
Total B.A.D.: 1.19 % no aggs

Debris: 5.29 %
Aggregates: 0.00 %
Modeled events: 8780
All cycle events: 8315
Cycle events per channel: 146
RCS: 3.896

C.

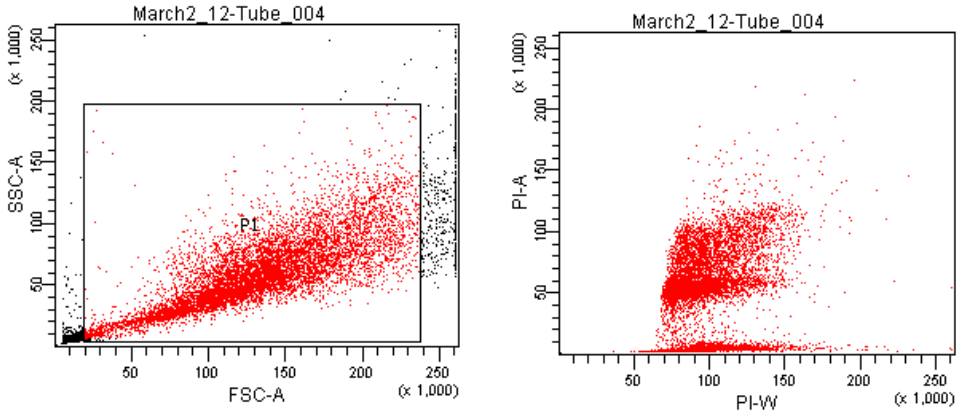

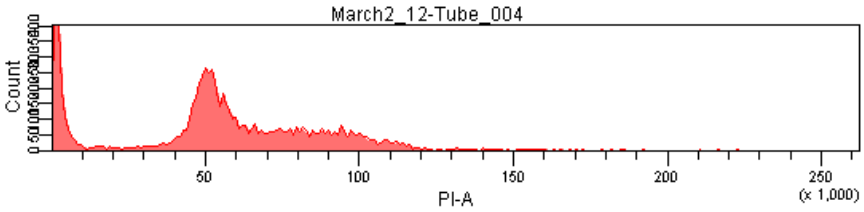

Tube: Tube_004

Population	#Events	%Parent	%Total
All Events	10,000	####	100.0
P1	8,605	86.1	86.1

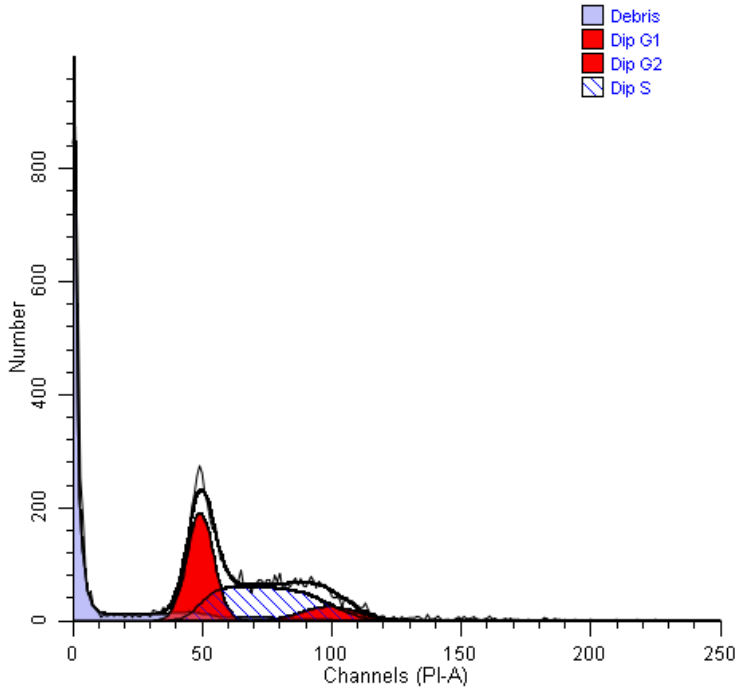

File analyzed: March2_12_Tube_004.fcs
Date analyzed: 2-Mar-2012
Model: 1Dn0n_DSD
Analysis type: Manual analysis

Ploidy Mode: First cycle is diploid

Diploid: 100.00 %
Dip G1: 40.48 % at 49.62
Dip G2: 10.71 % at 99.23
Dip S: 48.81 % G2/G1: 2.00
%CV: 10.28

Total S-Phase: 48.81 %
Total B.A.D.: 5.74 % no aggs

Debris: 31.61 %
Aggregates: 0.00 %
Modeled events: 8752
All cycle events: 5985
Cycle events per channel: 118
RCS: 1.962

D.

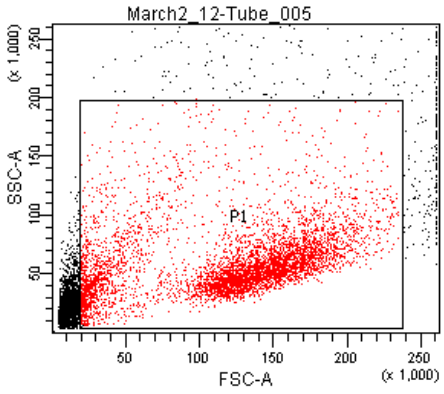

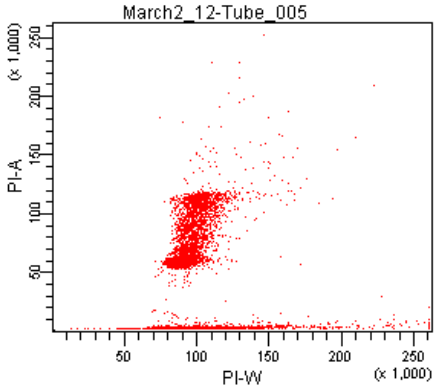

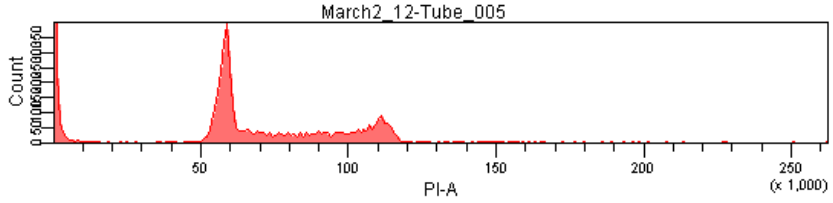

Tube: Tube_005

Population	#Events	%Parent	%Total
All Events	10,000	####	100.0
P1	5,296	53.0	53.0

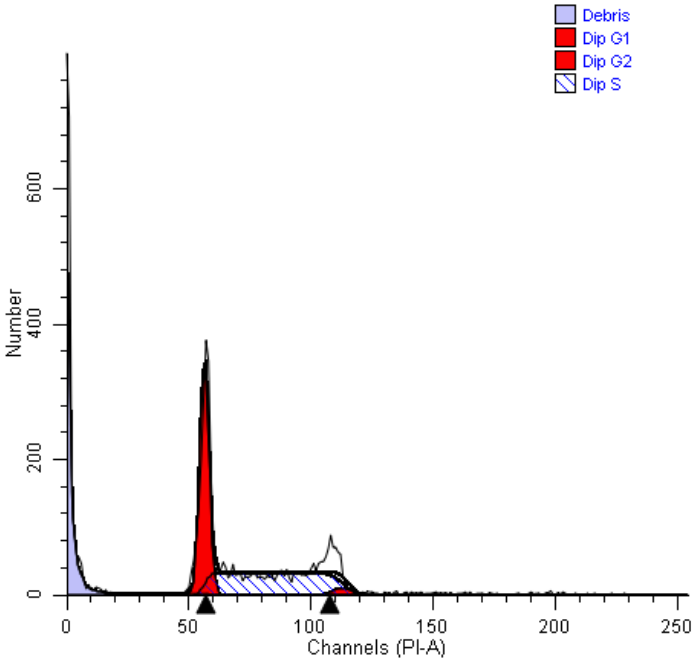

File analyzed: March2_12_Tube_005.fcs
Date analyzed: 2-Mar-2012
Model: 1Dn0n_DSD
Analysis type: Manual analysis

Ploidy Mode: First cycle is diploid

Diploid: 100.00 %
Dip G1: 45.81 % at 56.65
Dip G2: 2.59 % at 113.31
Dip S: 51.60 % G2/G1: 2.00
%CV: 3.37

Total S-Phase: 51.60 %
Total B.A.D.: 1.76 % no aggs

Debris: 25.09 %
Aggregates: 0.00 %
Modeled events: 4668
All cycle events: 3497
Cycle events per channel: 61
RCS: 2.826

E.

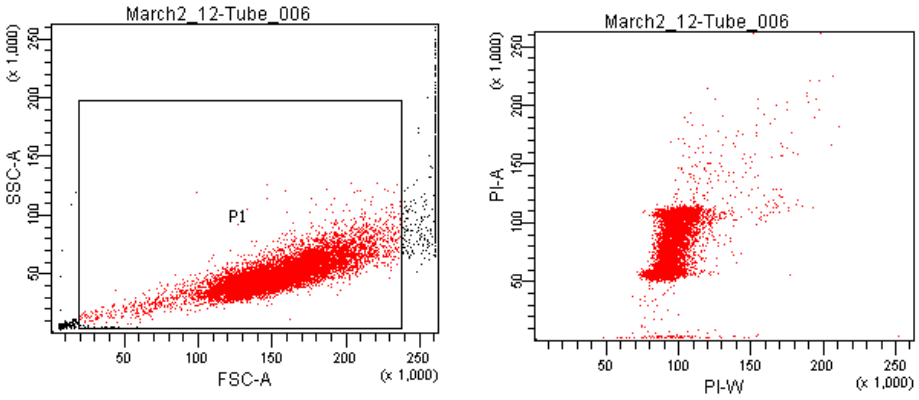

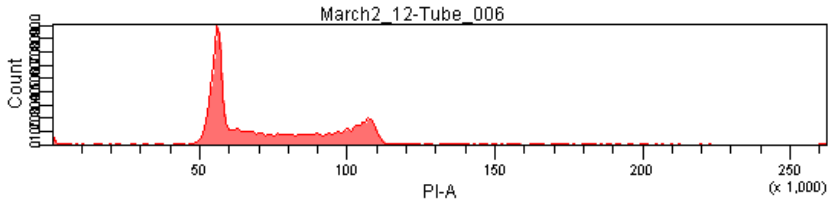

Tube: Tube_006

Population	#Events	%Parent	%Total
All Events	10,000	####	100.0
P1	9,207	92.1	92.1

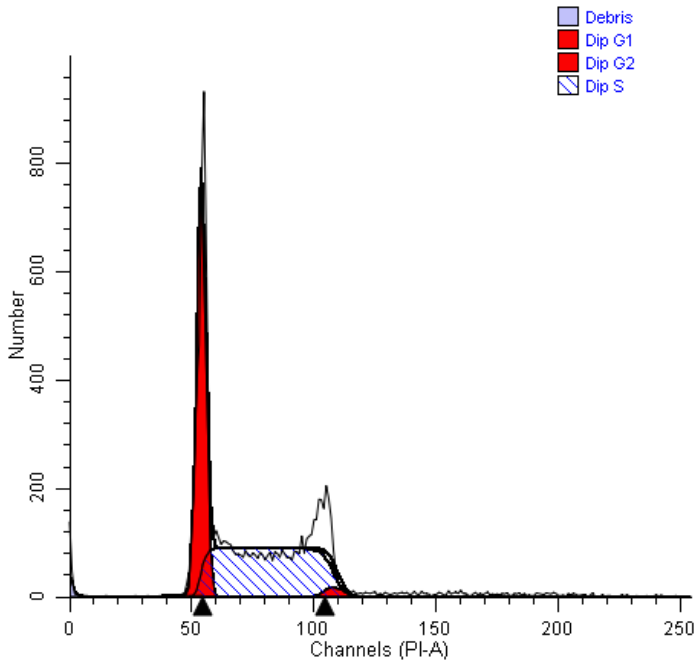

File analyzed: March2_12_Tube_006.fcs
Date analyzed: 2-Mar-2012
Model: 1Dn0n_DSD
Analysis type: Manual analysis

Ploidy Mode: First cycle is diploid

Diploid: 100.00 %
Dip G1: 41.67 % at 54.16
Dip G2: 1.89 % at 108.32
Dip S: 56.44 % G2/G1: 2.00
%CV: 3.44

Total S-Phase: 56.44 %
Total B.A.D.: 0.65 % no aggs

Debris: 1.95 %
Aggregates: 0.00 %
Modeled events: 8674
All cycle events: 8505
Cycle events per channel: 154
RCS: 5.419

F.

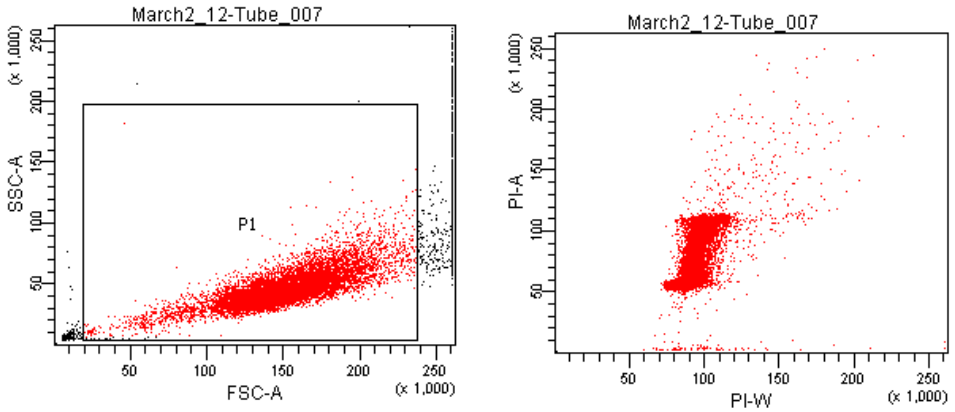

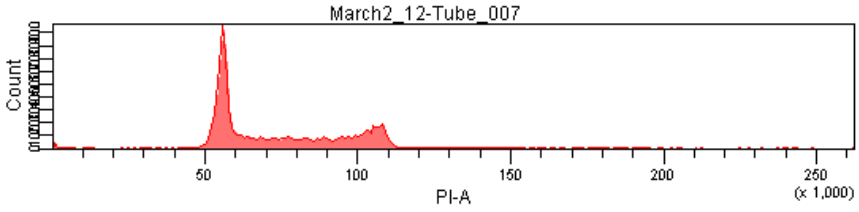

Tube: Tube_007

Population	#Events	%Parent	%Total
All Events	10,000	####	100.0
P1	8,830	88.3	88.3

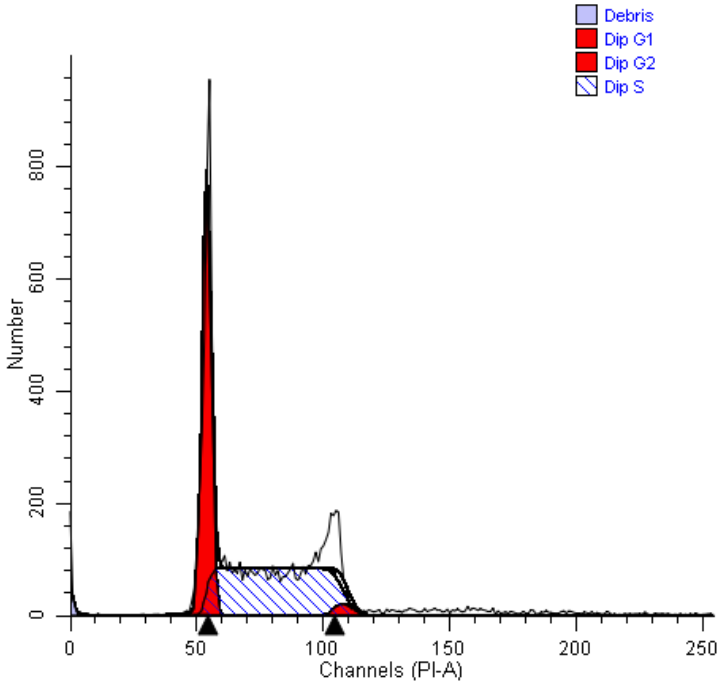

File analyzed: March2_12_Tube_007.fcs
Date analyzed: 2-Mar-2012
Model: 1Dn0n_DSD
Analysis type: Manual analysis

Ploidy Mode: First cycle is diploid

Diploid: 100.00 %
Dip G1: 41.68 % at 54.18
Dip G2: 2.20 % at 108.35
Dip S: 56.12 % G2/G1: 2.00
%CV: 3.28

Total S-Phase: 56.12 %
Total B.A.D.: 0.68 % no aggs

Debris: 2.14 %
Aggregates: 0.00 %
Modeled events: 8372
All cycle events: 8193
Cycle events per channel: 148
RCS: 6.144

APPENDIX B

Raw data for a sample apoptosis/necrosis flow cytometry in HT-29. HT-29 cells were plated and incubated for 24 h after which they were treated and incubated for an additional 48 h. Propidium iodide and annexin V alexafluor647 staining was performed and 10,000 cell samples were analyzed by flow cytometry. The graph in the upper left shows forward scatter (x-axis) and side scatter (y-axis) for the given cells. The parent population was selected from this graph as the counts most likely to be whole cells. The graph on the upper right shows PS exposure detected at 647 nm (x-axis) and PI permeabilization (y-axis) of the parent population. The population percentages used for Figure 6 are shown in the center of the page. The bottom graphs show the PI permeabilization (x-axis, upper) and PS exposure detected at 647 nm (x-axis, lower) verses cell count (y-axis). A. Untreated cells (tube 4); B. Vehicle control (0.1% DMSO) treated cells (tube 5); C. 10 μM camptothecin treated cells (tube 6); D. 25 μM MAP-870 treated cells (tube 7); E.10 μM MAP-870 treated cells (tube 8).

A

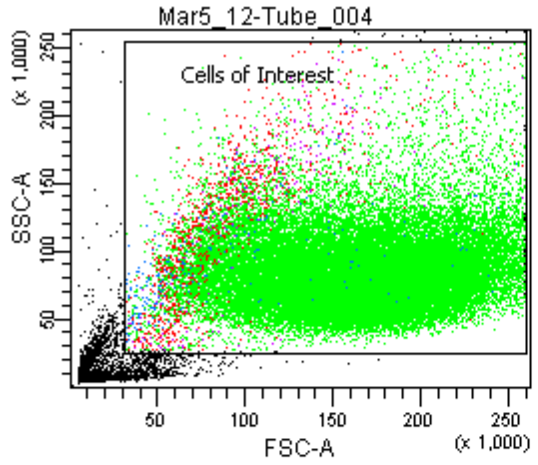

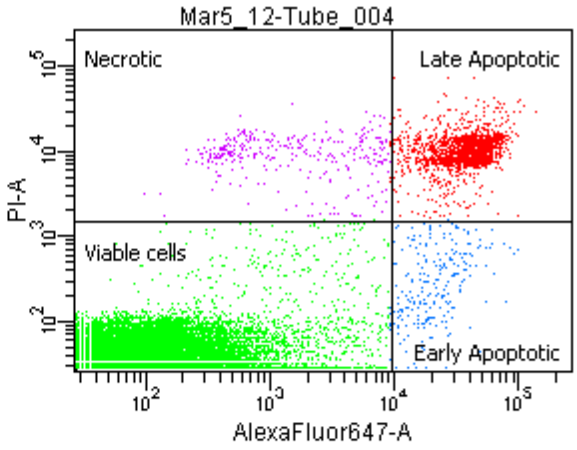

Tube: Tube_004

Population	#Events	%Parent	%Total
All Events	50,000	####	100.0
Cells of Interest	43,649	87.3	87.3
Necrotic	344	0.8	0.7
Late Apoptotic	1,708	3.9	3.4
Viable cells	41,353	94.7	82.7
Early Apoptotic	244	0.6	0.5

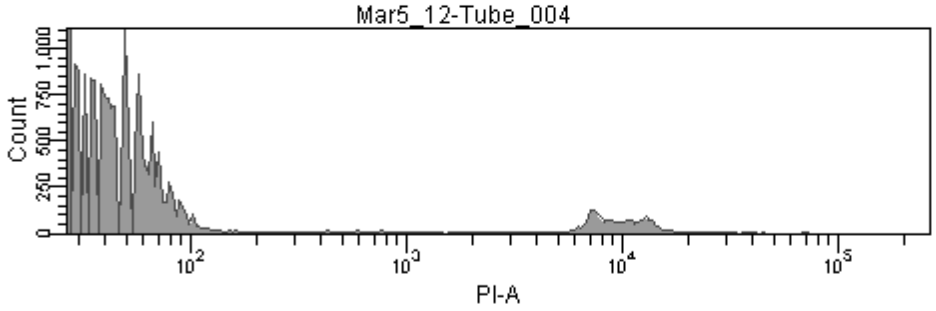

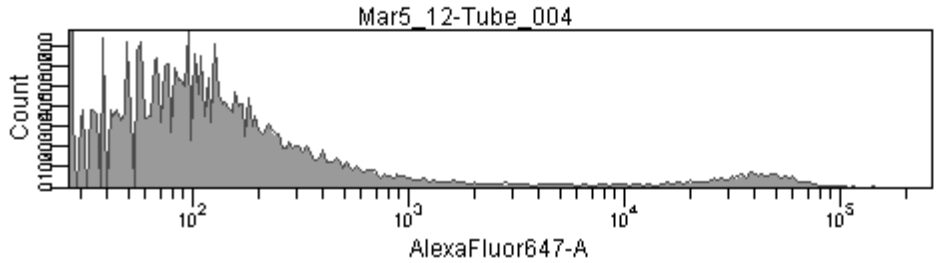

B

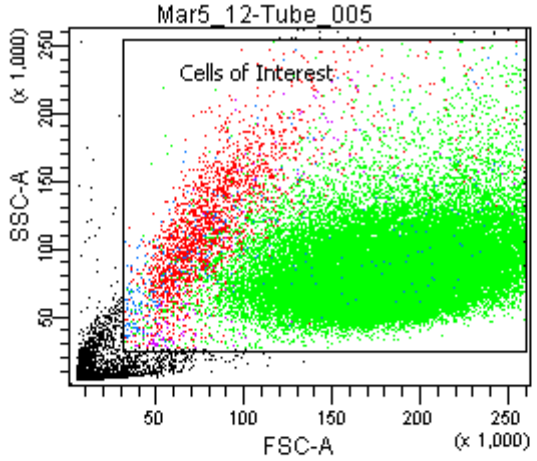

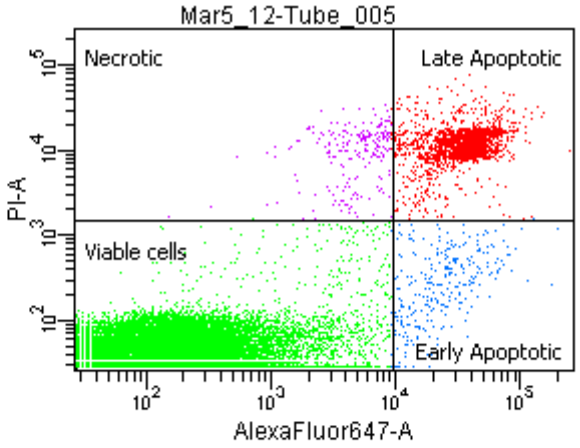

Tube: Tube_005

Population	#Events	%Parent	%Total
All Events	50,000	####	100.0
Cells of Interest	43,296	86.6	86.6
Necrotic	220	0.5	0.4
Late Apoptotic	2,273	5.2	4.5
Viable cells	40,507	93.6	81.0
Early Apoptotic	296	0.7	0.6

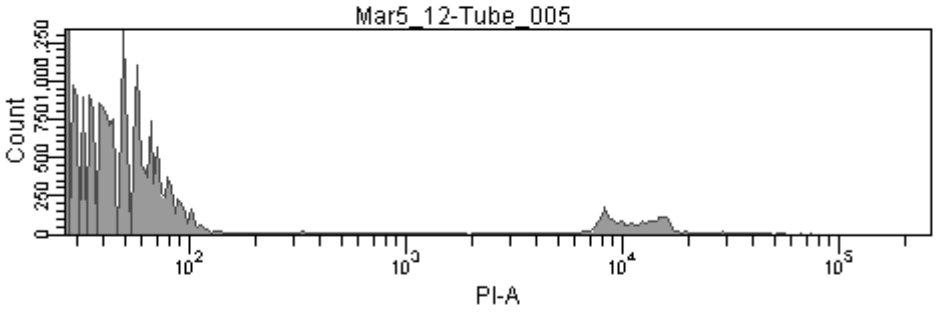

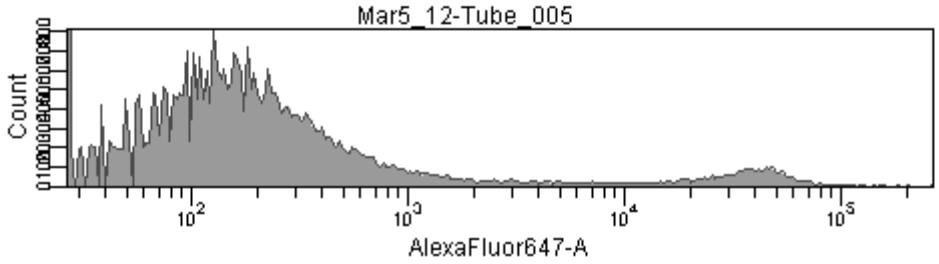

C

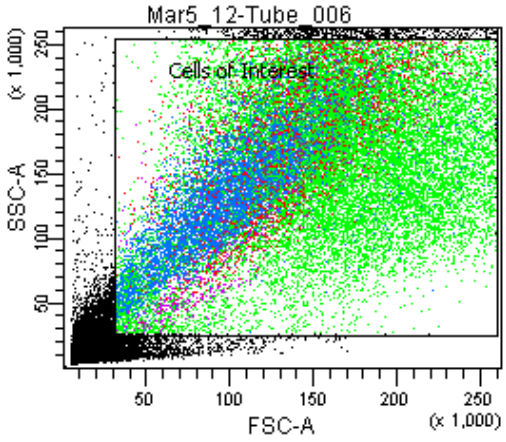

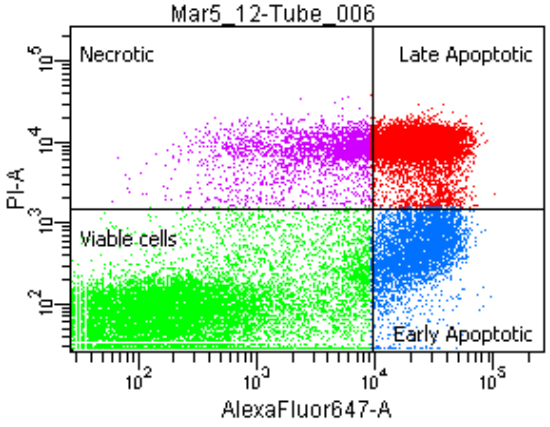

Tube: Tube_006

Population	#Events	%Parent	%Total
All Events	50,000	####	100.0
Cells of Interest	30,477	61.0	61.0
Necrotic	2,387	7.8	4.8
Late Apoptotic	6,693	22.0	13.4
Viable cells	16,902	55.5	33.8
Early Apoptotic	4,495	14.7	9.0

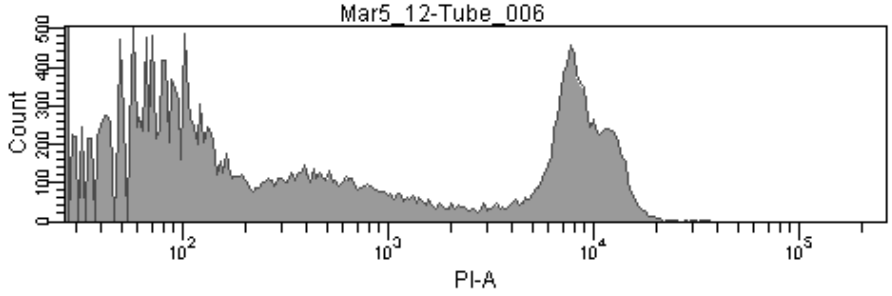

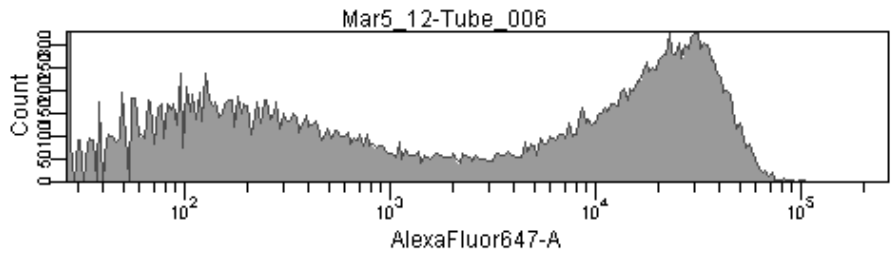

D

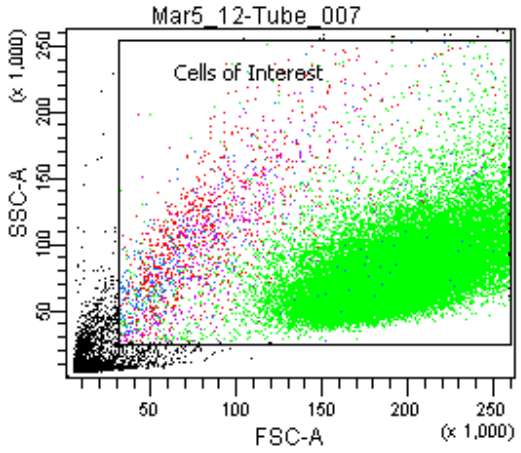

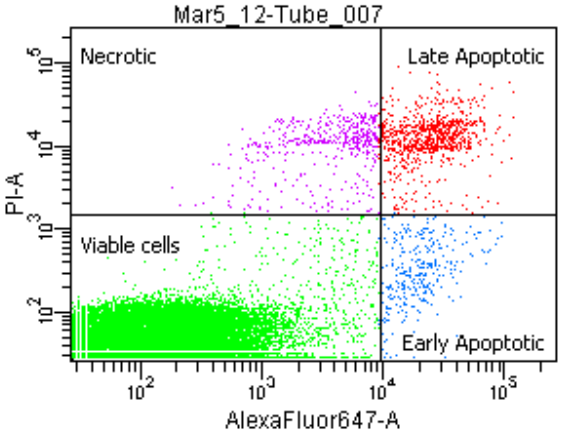

Tube: Tube_007

Population	#Events	%Parent	%Total
All Events	50,000	####	100.0
Cells of Interest	42,304	84.6	84.6
Necrotic	477	1.1	1.0
Late Apoptotic	884	2.1	1.8
Viable cells	40,618	96.0	81.2
Early Apoptotic	325	0.8	0.6

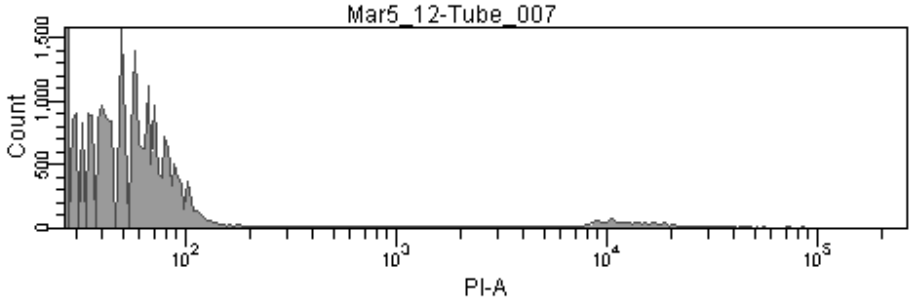

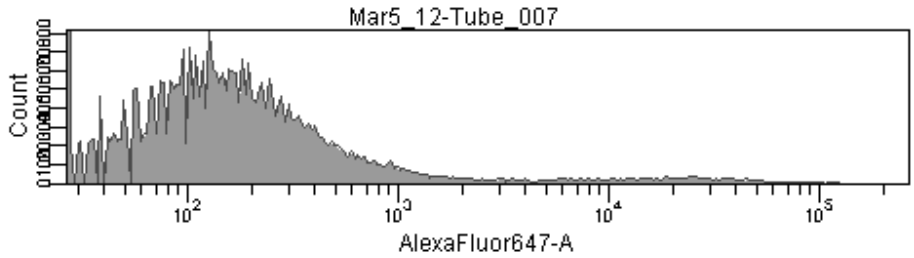

E

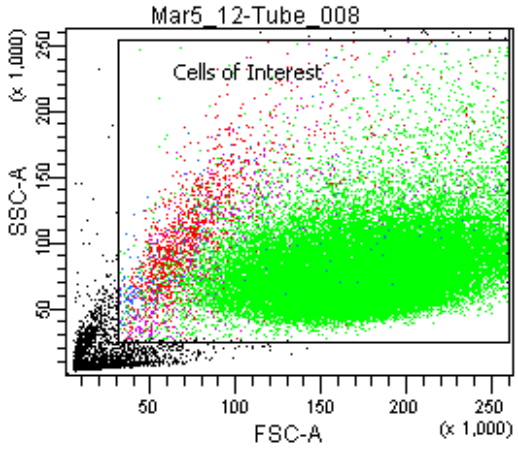

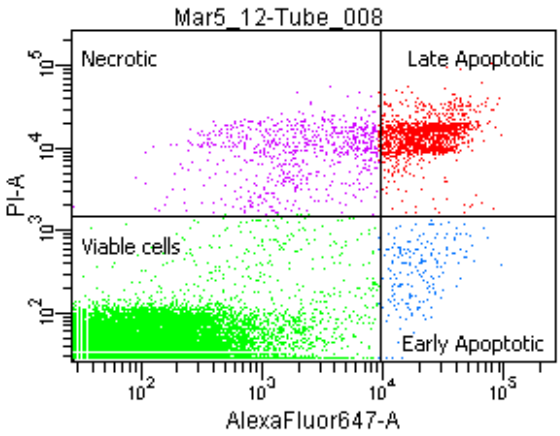

Tube: Tube_008

Population	#Events	%Parent	%Total
All Events	50,000	####	100.0
Cells of Interest	43,890	87.8	87.8
Necrotic	702	1.6	1.4
Late Apoptotic	1,407	3.2	2.8
Viable cells	41,590	94.8	83.2
Early Apoptotic	191	0.4	0.4

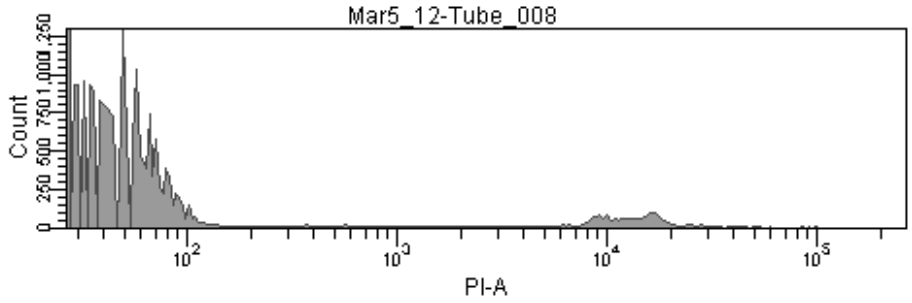

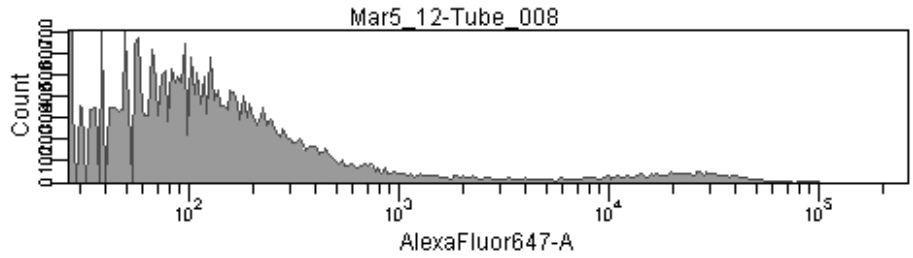

APPENDIX C

DNA fragmentation

Caspases are normally seen in type I PCD, but type I PCD can be caspase independent. In an effort to corroborate the data shown in the above Caspase-Glo3/7 assay a DNA laddering assay was attempted (data not shown). Apoptotic cells cleave their own DNA in regular patterns, which results in an effect known as laddering which can be viewed on an agarose gel. An example of an inconclusive positive control laddering assay for cells treated with 10 μM camptothecin is shown below. The data from these experiments were inconclusive; probably because the DNA isolation technique employed was inadequate possibly due to contaminating DNases. Alternatively, the inconclusive results below may be due to RNA contamination where the bands of interest would be expected (180-250 bp), which could have been better resolved if the samples were treated with DNase-free RNase. In the future, to overcome these problems a commercial DNA laddering assay kit is recommended.

Cells were treated with 10 μM MAP-870 for 48 hours and cells were rinsed with PBS, then trypsinized with 0.05% trypsin (Gibco) and centrifuged at 300 x g for 5 minutes. The cell pellet was treated using DNA-STAT (Tel-Test, Inc.) to isolate the DNA. The cells were homogenated with 800 μL of DNA-STAT then mixed and incubated for 5 minutes at RT. DNA was extracted by adding 160 μL of chloroform and allowing to stand for 2-3 minutes. The samples were vortexed and allowed to stand at RT for 5 minutes, then centrifuged at 12,000 g for 15 minutes at 4 ºC. The DNA-containing upper layer (600 μL) was removed, and the DNA was precipitated by adding 500 μL of isopropanol, and centrifuging at 12,000 g for 5 minutes at 4 ºC. The isopropanol was decanted, and the DNA pellet was washed with 1 mL of ice cold 75% ethanol and centrifuged at 12,000 g for 5 minutes at 4 ºC. The DNA samples were dissolved in 20 μL of RNase/DNase free water (invitrogen). A 0.7% agaraose gel was prepared in TBE with EtBr using standard protocol, and 10 μL of the DNA samples were added to 2 μL of 6x DNA loading dye (Thermo). These samples, and a GeneRuler 1 kb DNA ladder (Thermo) were loaded on the gel, and it was run at 25 V for 64 h, and visualized with UV light.

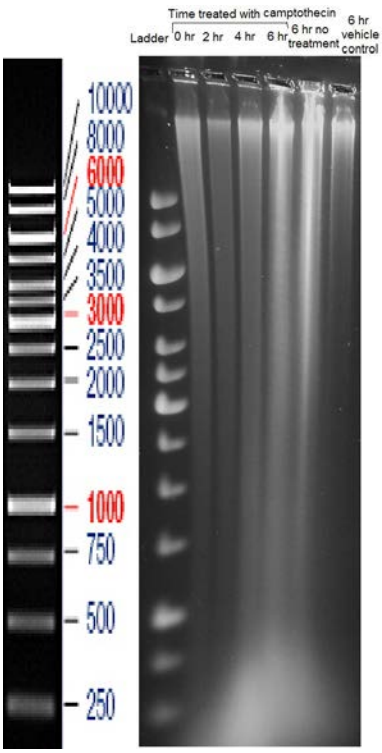
Time treated with camptothecin
Ladder
0 hr
2 hr
4 hr
6 hr
6 hr no treatment
6 hr vehicle control
10000
8000
6000
5000
4000
3500
3000
2500
2000
1500
1000
750
500
250